Title: Cortical granularity shapes information flow to the amygdala and its striatal targets in nonhuman primate

Abbreviated Title: Cortical granularity shapes information flow

McHale, AC[1]; Cho, YT[3], *Fudge, JL[1, 2]

University of Rochester, School of Medicine and Dentistry, Departments of Neuroscience[1] and Psychiatry[2], Rochester NY 14642; Yale University, Child Study Center and Department of Psychiatry, New Haven CT 06511[3]

*Correspondence to:
Julie L. Fudge, M.D.
Departments of Neuroscience, and Psychiatry
The Del Monte Institute for Neuroscience
University of Rochester Medical Center
julie_fudge@urmc.rochester.edu

Number of pages: 44
Number of figures: 13 (including 2 “extended data” figures)
Number of tables: 1
Number of words for abstract: 250 words
Number of words for introduction: 642 words
Number of words for discussion: 1470 words
Conflict of interest statement: The authors declare no competing financial interests.
Acknowledgements: This work was funded through the support of the National Institutes of Mental Health R01MH63291 (J.L.F.), and the Schmitt Program on Integrative Neuroscience (SPIN) GR504304 (J.L.F.). We thank Nanette Alcock for assistance with histology and immunocytochemistry. We also thank Keshov Sharma for R code advice and helpful discussions about data analysis.

Abstract

The prefrontal cortex (PFC) and insula, amygdala, and striatum form interconnected networks that drive motivated behaviors. We previously found a connectional trend in which granularity of the ventromedial and orbital PFC/insula predicted connections to the amygdala and also the scope of amygdalo-striatal efferents, including projections beyond the 'classic' ventral striatum. To further interrogate this triad and define the 'limbic (amygdala-recipient) striatum', we conducted tract tracing studies in two cohorts of primates to define the scope of cortico-amygdalo-striatal (indirect) and cortico-'limbic' striatal (direct) paths originating in the entire PFC and insula. With larger data sets and a quantitative approach, we found that the level of cortical granularity predicts the complexity and location of projections to both the amygdala and striatum. Remarkably, 'cortical-like' basal nucleus subdivisions also followed these rules in their projections to the striatum. In both 'direct' and 'indirect' paths to the 'limbic' striatum, agranular cortices formed a 'foundational', broad projection, and were joined by inputs from progressively more differentiated cortices. In amygdalo-striatal paths, the ventral basal nucleus was the 'foundational' input, with progressively more dorsal basal nucleus regions gradually adding inputs as the 'limbic striatum' extended caudally. Together, the 'indirect' and 'direct' paths follow consistent rules dictating projection strength and complexity to their targets. In the 'indirect' path, the agranular 'interoceptive' cortices consistently dominate amygdala inputs to the striatum. In contrast, 'direct' cortical inputs to the 'limbic' (amygdala-recipient) striatum create gradual shifts in connectivity fingerprints to provide clues to functional differences in the classic versus caudal ventral 'limbic' striatum.

Significance Statement

The 'limbic system' broadly refers to brain circuits that coordinate emotional responses. Here, we investigate circuits of the amygdala, which is involved in coding the emotional value of external cues, and their influence on the striatum. Regions of prefrontal cortex and insula form gradients of overlapping inputs to basal nucleus of the amygdala, which are fed forward to the striatum. Direct cortical inputs to these 'amygdala-recipient' striatal areas are surprisingly organized according to similar principles, but subtly shift from the classic ventral striatum to the caudal ventral striatum. Together, these distinct subsystems—cortico-amygdala-striatal circuits and direct cortico-striatal circuits—provide substantial opportunity for different levels of internal, sensory, and external experiences to be integrated within the striatum, a major motor-behavioral interface.

Introduction

The prefrontal cortex (PFC) and insula, amygdala, and striatum form interconnected networks that drive motivated behaviors (Van Hoesen et al., 1981; Yeterian et al., 2012). Specific cortical regions project to the amygdala, modulating amygdala neural responses (Klavir et al., 2013; Likhtik et al., 2014). At the same time, these cortical regions and the amygdala form uni-directional inputs to the striatum to mediate goal-directed responses (Haber and Knutson, 2010). This 'triadic' circuitry is implicated in human neuropsychiatric diseases (Akil et al., 2018; Ressler, 2020). Yet, organizational principles of this classic 'limbic' triad are still not completely understood at the cellular level in nonhuman primate brain.

Although they are separate lobes of cortex, the PFC and insula share a progressive change in cortical laminar differentiation (Mesulam and Mufson, 1982; Barbas and Pandya, 1989). The degree of 'granularity' across the cortical mantle generally refers to the relative presence or absence of 'granular cell' layer IV (Brodmann, 1909; Carmichael and Price, 1994; Petrides and Pandya, 1999, 2002). "Agranular" cortex lacks a granular layer IV, "dysgranular" cortex has an incompletely developed layer IV, and "granular" cortex has a well-differentiated layer IV. Within these broad categories, incremental changes in laminar organization exists, leading to gradual shifts from agranular to dysgranular to granular across the cortical mantle. Classic subdivisions of the PFC and the insula are therefore not independent regions, but rather reflect this continuous laminar organization (Barbas and Garcia-Cabezas, 2016).

The basal nucleus of the amygdala is a key recipient of top-down inputs from the PFC and insula, and is a major output to the striatum (Carmichael and Price, 1995; Ghashghaei and Barbas, 2002; Cho et al., 2013). This nucleus is expanded in primates (Stephan et al., 1987), and has an increased cytoarchitectural complexity along its dorsal-ventral axis. In monkey and human, three large subdivisions of the basal nucleus are recognized: the magnocellular (Bmc), intermediate (Bi,) and parvicellular (Bpc). As their names imply, these dorsally-to-ventrally arranged basal nucleus subdivisions are distinguished by pyramidal cell size and packing density (Braak and Braak, 1983).

Amygdala inputs are a defining input to the 'classic' ventral striatum, which is involved in forming goal-directed behaviors (Robbins et al., 1989; Popescu et al., 2009). Prior work however has demonstrated amygdala projections extend past the 'classic' ventral striatum into caudal aspects of the striatum, which we term the ‘caudal ventral striatum’ (Russchen et al., 1985; Fudge et al., 2002; Cho et al., 2013).

In a previous study, examining ‘cortico-amygdalo-striatal’ paths limited to the ventromedial and orbital PFC and insula, we found evidence that relatively higher levels of laminar organization in cortico-amygdala projections governed the topography of cortico-amygdala paths, and was also related to the extent of projections in the next limb of the circuit, the amygdalo-striatal path (Cho et al., 2013). Findings from this study raised subsequent questions around whether the most differentiated dorso-lateral regions of the PFC and insula followed this topography of inputs, and how the topography of cortico-

amygdala-striatal circuits compared to the topography of direct cortico-striatal circuits in striatal regions receiving amygdala input.

Here, we took a systems-based approach to quantitatively compare the organization of 'indirect' cortico-amygdala-striatal circuits and 'direct' cortico-striatal circuits in striatal regions receiving amygdala inputs. We first examined the entire extent of the 'indirect' path, using multiple small injection sites of bi-directional tracer focused on the specific basal nucleus subregions. In the second set of experiments, we placed small injections of retrograde tracer into territories of 'limbic' (amygdalo-recipient) striatum defined by the first cohort, and compared whether direct cortical-'limbic' striatal paths followed similar connectivity principles as indirect paths. Remarkably, we found that a recursive set of hierarchically organized connections, governed by cortical granularity, dictate both the direct and indirect cortical paths to the 'limbic' striatum. This organization resulted in unique connectional 'fingerprints' in subregions of the basal nucleus of the amygdala and the 'limbic' (amygdala-recipient) striatum, suggesting functional differences.

Materials and Methods

Study design. Two cohorts of *Macaca fascicularis* were used for this study (Labs of Virginia, Three Springs Laboratories, and Worldwide Primates) (Fig. 1). In the first cohort (Cohort 1), a bidirectional tracer injection was placed in various subdivisions of the basal nucleus of the amygdala. Portions of these data were previously published (Cho et al., 2013). To examine the cortico-amygdalo-striatal circuit, we charted and analyzed the number of retrogradely labeled cells in the PFC/insula, and the distribution of

anterogradely labeled fiber terminals in the striatum. In the second cohort (Cohort 2), we used anterograde tracing maps from Cohort 1 as a guide for placing retrograde tracer injections into the 'limbic' striatum (defined as striatal regions receiving amygdala input). Retrogradely labeled cells in the PFC/insula and in the amygdala were then charted, quantified, and analyzed.

Surgical procedures and tissue preparation. All surgeries were approved by the University of Rochester Committee on Animal Research and follow the National Institutes of Health guidelines. To conserve animals, Cohort 1 data includes new analyses in some previously mapped cases (Fudge et al., 2004; Fudge et al., 2005; Cho et al., 2013; Decampo and Fudge, 2013), as well as new cases. A total of 13 animals weighing between 3.3 kg and 9.3 kg were used across both studies (Male n = 12; Female n = 1). To determine surgical coordinates, some animals had an individualized MRI T2 scan prior to surgery; others had intra-operative electrophysiologic mapping (Fudge et al., 2004; Fudge et al., 2005; Cho et al., 2013; Decampo and Fudge, 2013).

Monkeys that underwent individualized MRI T2 scans were first administered an intramuscular injection of ketamine (10 mg/kg), then intubated with isofluorane gas during the scanning process. Three days prior to stereotactic surgery, the animals received daily prophylactic pain control with gabapentin (oral dose), which was maintained for 3 days post-operatively. On the day of surgery, monkeys were administered an intramuscular injection of ketamine (10 mg/kg), intubated, and then administered either intravenous pentobarbital (initial dose, 20 mg/kg, i.v.) (animals undergoing electrophysiologic

mapping) or isofluorane gas anesthesia. Once monkeys were placed in a stereotactic head frame, a craniotomy was performed under sterile conditions. For some animals, electrophysiological mapping was conducted first, and electrophysiological features of cells were noted during several penetrations. Injection sites were then plotted for subsequent tracer injections.

For Cohort 1, the basal nucleus was pressure-injected at various dorsoventral and rostrocaudal sites with either 40 nl of the bidirectional tracers Lucifer yellow conjugated to dextran amine (LY; Invitrogen), Fluorescein conjugated to dextran amine (FS; Invitrogen), or Fluoro-Ruby (tetramethylrhodamine) conjugated to dextran amine (FR; Invitrogen). Antibodies to these tracers do not cross-react, and have similar retrograde and anterograde properties, making them suitable for simultaneous use within the same animal, based on our previous work (Haber et al., 2000; Fudge et al., 2002). For Cohort 2, one striatal site per animal was pressure-injected with 40 nl of wheat germ agglutinin conjugated to horseradish peroxidase (WGA-HRP; Sigma). Following all surgeries, the bone flap was replaced and the overlying tissue sutured. For both cohorts, animals were deeply anesthetized and sacrificed via intracardiac perfusion 10 to 12 days after surgery [0.9% saline solution containing 0.5 ml of heparin sulfate followed by cold 4% paraformaldehyde in 0.1M phosphate buffer (PB (0.1M PO_4 pH 7.2)) and 30% sucrose solution for 1 hr)]. After overnight postfixation, brains were cryoprotected in increasing concentrations of sucrose solution (10%, 20%, and 30%). Brains were sectioned coronally on a freezing, sliding microtome at 40 µm, placed in 24 consecutive compartments containing cold cryoprotectant solution (30% sucrose and 30% ethylene

glycol in PB), then stored at -20°C (Rosene et al., 1986).

Histology

Immunohistochemistry (ICC). In both Cohorts, every eighth section through the entire brain was processed using ICC for the relevant tracer. In Cohort 1, adjacent sections through the striatum were processed for calbindin-D28k protein (CaBP) in order to localize the position of anterogradely labeled fibers in striatal subregions (see *Amygdalo-striatal path* section in *Cortico-amygdalo-striatal analyses*; **Cohort 1**). In Cohort 2, CaBP-immunoreactivity (IR) in adjacent sections was used to localize tracer injections within striatal subregions (see *Amygdalo-striatal path;* **Cohort 2**). For all experiments, tissue was rinsed in phosphate buffer with 0.3% Triton-X (PB-TX) overnight. The next day, brain slices were treated with an endogenous peroxidase inhibitor for 5 minutes, and then underwent more rinses in PB-TX. Sections were then pre-incubated for 30 minutes in 10% normal goat serum blocking solution with PB-TX (NGS-PB-TX). All sections were then incubated in primary antisera to LY (1:2000; Invitrogen, rabbit), FS (1:2000; Invitrogen, rabbit), FR (1:1000; Invitrogen, rabbit), WGA (1:2500-1:7500 depending on dilution curve; Sigma, rabbit), or CaBP (1:10,000; Millipore Bioscience Research Reagents, mouse) at 4°C for four nights. Sections were then thoroughly rinsed, again blocked with 10% NGS-PB-TX, and incubated for 40 minutes in the appropriate biotinylated secondary antibody. After more rinses, sections with bound anti-LY, anti-FR, anti-FS, anti-WGA, or anti-CaBP antibodies were incubated in an avidin-biotin complex (Vectastain ABC kit; Vector Laboratories), and visualized with 3,3'- Diaminobenzidine (DAB), activated with 0.3% hydrogen peroxide (H_2O_2).

Cresyl Violet. In order to localize cortical cytoarchitectonic boundaries for each animal (both Cohorts 1 and 2), we stained 1:24 adjacent or near-adjacent sections for each case with cresyl violet (Chroma-Gesellschaft, West Germany).

Acetylcholinesterase (AChE). In Cohort 1, AChE staining in adjacent sections was used to identify injection site location in the basal nucleus, while in Cohort 2, AChE staining was used to localize tracer-labeled neurons in specific basal nucleus subdivisions. For both, we stained 1:24 adjacent or near-adjacent sections for AChE, using the Geneser-Jensen technique (Geneser-Jensen and Blackstad, 1971).

Analysis:

Cytoarchitectural criteria for the PFC and insula (Fig. 2)

The PFC is defined as the frontal lobe anterior to the arcuate sulcus. Within the PFC, we define the ventromedial and orbital subdivisions according to the nomenclature of Carmichael and Price (Carmichael and Price, 1994), and the dorsomedial (dmPFC) and dorsolateral (dlPFC) and ventrolateral (vlPFC) subdivisions according to Petrides et al. (Petrides and Pandya, 1999, 2002). Insula subdivisions were defined according to Carmichael and Price (Carmichael and Price, 1994). Regardless of nomenclature, all cytoarchitectural maps of the PFC recognize the gradual transition from agranular to granular laminar organization in the basoventral and mediodorsal direction, based on laminar complexity and the relative development of layer IV (Brodmann, 1909; Preuss and Goldman-Rakic, 1991; Barbas, 2007; Nieuwenhuys et al., 2007). The insula similarly

226 progresses from agranular to granular, but in a rostroventral to caudodorsal direction
227 (Mesulam and Mufson, 1982). See Supplemental Methods for detailed descriptions of
228 laminar characteristics of Brodmann's areas.
229
230 *Categorization of cortical regions by architecture*
231 For quantitative analysis, we categorized cortical areas into either 3 (general) or 9
232 (refined) categories of cortical hierarchy, based on examining layer IV thickness (for 3
233 category granularity) and the extent of layer V sublamination (for 9 category granularity)
234 under Nissl stain (Carmichael and Price, 1994) (Table 1). For 3 category granularity,
235 cortical regions were categorized as agranular cortex if they did not have layer IV,
236 dysgranular if they had incompletely developed layer IV, and granular if they had
237 completely developed layer IV.
238
239 ***Cohort 1.***
240 *Injection site placement.* Relative injection site placement within the Bmc, Bi, and Bpc
241 was determined using adjacent AChE sections for each animal. Throughout the
242 rostrocaudal extent of the basal nucleus, the Bmc is darkly stained with AChE, the Bi has
243 intermediate AChE staining, and the Bpc is lightly stained with AChE, corresponding to
244 the cytoarchitectural gradients in the nucleus (Amaral and Bassett, 1989). All nuclei, and
245 specifically basal nucleus subdivisions, were traced along with landmarks, such as blood
246 vessels across sections, and aligned over tracer-labeled sections in Adobe Illustrator
247 Creative Suite (CS).
248

Cases with tracer leakage into overlying structures or white matter tracts were not included in the analysis. To confirm our assessment of injection site placement, we also examined the pattern of retrograde labeling in brain regions known to be a source of afferents to each subdivision. For example, the Bmc receives inputs from the inferotemporal cortex (Herzog and Van Hoesen, 1976), while the Bpc does not; the Bpc receives inputs from the hippocampus in contrast to the Bi and Bmc (Saunders et al., 1988; Fudge et al., 2012).

Cortico-amygdalo-striatal analyses

Cortico-amygdala path. Retrogradely labeled cells in 1:24 sections were charted through the entire rostral-caudal extent of the PFC and insula using an Olympus AX70 microscope interfaced with Neurolucida, via a video CCD (Microbrightfield, Williston, VT). Cytoarchitectural boundaries of cortex using traditional nomenclature were determined on adjacent Cresyl violet-stained sections under the microscope. These labeled charts were then aligned onto maps of retrogradely labeled cells in Adobe Illustrator CS. The number of retrogradely labeled cells in each cortical subdivision was counted using the Adobe Illustrator "objects" count feature. Cortical regions for each region were then categorized into 3- and 9-category "agranular", "dysgranular", and "granular" groupings as described above (Table 1).

After assignment of each cortical area to a cortical granularity category, we used the "*circlize"* package in R (R Foundation for Statistical Computing, Vienna, Austria) to generate chord diagrams of our retrograde cortical data, using our 3 and 9 category

272 classifications of cortical granularity (Gu et al., 2014). Chord diagrams are an effective
273 way to visualize the directionality and connectivity between different nodes of a data set.
274 'Fragments', which represent each node, are found along the outer perimeter of the plot.
275 Color-coded chords display the directionality and strength of connections between
276 'fragments'. If the color of a chord and a 'fragment' are the same, this indicates how that
277 'fragment' is connected to other nodes in the data set (i.e. how the agranular cortex
278 'fragment' projects into various basal nucleus injection site 'fragments'). Chord thickness
279 indicates the relative strength or weakness of connections between nodes (i.e. chord
280 thickness represents the number of retrogradely labeled cells originating from a
281 granularity 'fragment'). The small tic marks and numbers found along the axis of each
282 'fragment' indicate number of cells.
283
284 *Amygdalo-striatal path.* Anterogradely labeled terminal fibers were hand-charted through
285 the rostro-caudal extent of the striatum with the aid of a drawing tube under dark-field
286 illumination. Labeled thick fibers that did not contain boutons were considered fibers of
287 passage and were therefore not included. All hand-drawn charts were then scanned at
288 high resolution and converted in Adobe Illustrator CS for formatting. Striatal boundaries
289 were then determined through comparison to adjacent or near-adjacent CaBP-labeled
290 sections. CaBP-labeled sections were projected onto paper maps of anterogradely
291 labeled fibers in the striatum. Landmarks including blood vessels and fiber tracts were
292 carefully aligned, and CaBP-positive and CaBP-negative areas of the striatum were
293 drawn in. Maps were then scanned into digital format at high resolution, and converted
294 in Adobe Illustrator CS.

Cohort 2.

Injection site placement. Injection sites were targeted to the rostral ventral striatum, and also to regions of the ventromedial striatum posterior to the anterior commissure, based on anterograde maps from Cohort 1. Injection site position was determined with reference to adjacent CaBP-labeled sections. CaBP-poor regions were used to identify the 'shell' (Meredith et al., 1993; Fudge and Haber, 2002). All injection sites that resulted in retrogradely labeled cells in the amygdala were used for Cortico-'limbic' striatum and Amygdalo-striatal analyses.

Amygdalostriatal path. The location and quantification of retrogradely labeled cells in basal nucleus subdivisions was mapped in 1:24 sections, with reference to adjacent AChE stained sections. All retrogradely labeled cells in the amygdala were subsequently sorted by subdivision (Bmc, Bi, and Bpc) based on levels of AChE activity and cellular features, and analyzed with respect to position of the injection within the striatum.

Cortico-'limbic' striatal path. Only injection sites resulting in significant numbers of labeled cells in the basal nucleus (>10) were used for these analyses. We quantified retrogradely labeled cells in the entire PFC and insula, and applied the same criteria for classification, analysis, and visualization described for Cohort 1.

Comparing cortico-amygdala-striatal and cortico-striatal pathways. To first address whether amygdala neuronal populations projecting to different striatal regions received a

similar balance of agranular, dysgranular, and granular cortical inputs, we used a 'ratio of ratios' approach to examine data across Cohort 1 (cortico-amygdala) and Cohort 2 (amygdala-striatal). We first pooled the sum of all agranular, dysgranular, and granular labeled cell counts resulting from Bmc, Bi, and Bpc injection sites (i.e. cortico-amygdala data), and converted these sums into percentages. Only basal nucleus injection sites that were wholly confined to one of these subdivisions were used. Once the proportion of labeled neurons in the agranular, dysgranular, and granular cortex were determined for Bmc, Bi, and Bpc injection groupings, we multiplied these percentage values by the number of retrogradely labeled cells in Bmc, Bi, and Bpc resulting from each striatal injection site in Cohort 2. We then converted this sum into a final percentage value to assess the balance of agranular, dysgranular, and granular cortical inputs to amygdala-striatal projecting cells for each striatal site. We finally conducted bootstrap analysis to check the 'stability' of our final percentage values in 'indirect' pathway calculations. We did 4 replicates of the data, and found that the average difference of full versus bootstrap data was = 1.4%, the median was 1.0%, the SD was 0.01198, the maximum was 5.6%, and the minimum was 0.1%. The proportion of labeled cells in the agranular, dysgranular, and granular cortices for the indirect pathway (conjunction of Cohort 1 cortico-amygdala data and Cohort 2 amygdalo-striatal data) were then compared to the proportion of labeled cells in agranular, dysgranular, and granular cortices for each injection site associated with the direct cortico-striatal pathway (Cohort 2). Results were expressed as the proportion of labeled neurons in the agranular, dysgranular, and granular cortex associated with each path for each striatal injection site.

Results

Cortico-amygdalo-striatal paths (Cohort 1)

Basal nucleus injection site placement (Fig. 3). In the Bmc, there were three injections placed at slightly different levels—cases J12LY, J16LY, J12FR—as well as five injections at different levels of the Bpc—cases J20LY, J15LY, and J14FR in rostral Bpc, and cases J15FS and J14FS in caudal Bpc, all reported previously (Cho et al., 2013). Three new injections at slightly different levels of the Bi—cases J47FS, J44FR, and J52LY were made and assessed for a more complete survey of the basal nucleus subdivisions. The Bi injection in J47FS was the most ventral, the injection in J52LY extended slightly more dorsally, and the injection in J44FR was most dorsal and lateral, straddling the border with the lateral Bmc.

Cortical inputs along basal nucleus subdivisions (Fig. 4). After all injections in the basal nucleus, a general pattern emerged in which injection sites placed in the Bpc resulted in many labeled cells in the PFC and insula, restricted to the agranular PFC and insula, while increasingly dorsal and rostral injections in the Bpc, Bi, and Bmc resulted in labeled cells in broader cortical regions, as detailed below.

Bpc. Injection sites in the Bpc (cases J15FS, J14FS, J14FR, J20LY, J15LY) resulted in labeled cells largely confined to agranular cortex, i.e. area 25c, 14c, and agranular insula areas (Fig. 4A). J15FS and J15LY had the most labeled cells in agranular insula subdivisions Iapm and Ial, J14FS had most labeling in Iai and Iapl, J14FR had most labeling in Iapl, and J20LY had most labeling in Ial and Iapl. Across Bpc cases, the

majority of labeled cells was in the agranular insula rather than PFC, however, the proportion of labeled cells in the agranular PFC increased gradually as the injection sites were positioned more laterally. Case J15LY, which is an injection in the 'transition' between the Bpc and Bi, had additional labeling in agranular area 24a. J20LY had relatively more labeled cells in dysgranular insula compared to other Bpc sites.

Bi. Bi injections sites (cases J47FS, J52LY, and J44FR) resulted in the majority of labeled cells in agranular cortices, but with a relatively greater contribution of labeled cells in dysgranular and granular cortices compared to Bpc (Fig. 4A). Similar to Bpc, high numbers of labeled cells were found in 25c, 14c, and agranular insula. Case J47FS had the most labeled cells in Iapm and Iai, case J52LY had the majority of labeled cells in Iai and Ial, and case J44FR had the most labeled cell in Iapl. In contrast to Bpc sites, a broader distribution of labeled cells occupied relatively more differentiated agranular areas, including 32c, 24a, 24b, and 13a, as well as labeled cells in dysgranular regions such as area 13b. J44FR, located in a 'transition' region between Bi and Bmc, had relatively more labeled cells in agranular area 24c, dysgranular insula, and 8B, in addition to labeled cells specifically in granular areas 12l and 8Ad.

Bmc. While the majority of labeled cells remained in the agranular regions of PFC and insula, injections in Bmc cases (J12FR, J16LY, and J12LY) had the broadest distribution of labeled cells. Similar to Bpc and Bi, Bmc had many labeled cells in agranular areas 25c, 14c, and agranular insula. Similar to Bi cases, Bmc cases had high levels of labeled cells in agranular areas 24a, 24b, and 24c, but in contrast, also had moderate numbers

of labeled cells in dysgranular areas 14r, 8B, 13m, and 12o, and some labeled cells in granular areas 45, 9, 8Ad, 8Av, and 46.

Quantitative analyses revealed that cortical granularity subtype, rather than association with the insula or PFC, predicted inputs across, and even within, basal nucleus subdivisions (Fig. 4B). The agranular cortices in both PFC and insula contained labeled cells after all basal nucleus injections, but were the sole contributor when injection sites were placed in the caudomedial Bpc. Labeled cells in dysgranular cortices appeared and increased in numbers following injections along the rostro-dorsal axis, from the rostro-medial Bpc to Bi to Bmc. Labeled cells in the granular cortices of the insula and PFC formed a relatively smaller contribution, seen only after injections in dorsal Bi and Bmc. The pattern of inputs was nested such that labeled cells in incrementally higher levels of cortical organization only appeared in conjunction with labeled cells in less differentiated cortical areas. Analyses using the more refined (9 category) granularity classification showed a similar, nested pattern (Fig. 4-1). In these, subcategories of differentiation within a general granularity 'level' were themselves overlapping in a hierarchical manner.

Basal nucleus-striatal path. The distribution and relative density of anterogradely labeled fibers in the striatum from each basal nucleus injection site were mapped (Fig. 5). While all injections sites in the basal nucleus subdivisions resulted in labeled fibers in the shell of the nucleus accumbens, the distribution of labeled fibers varied predictably, expanding its distribution in the striatum as injection site position moved from the caudomedial to rostro-dorsal basal nucleus.

Bpc. Caudomedial Bpc injections (Cases J14FS, J15FS) had labeled fibers largely confined to the dorsomedial shell of the ventral striatum, while more rostral and lateral Bpc injections (J20LY, J14FR, J15LY) resulted in additional labeled fibers in the medial and lateral shell of the ventral striatum, interstitial nucleus of the anterior commissure (IPAC, or fundus striatii), and a small region of the caudomedial putamen caudal to the anterior commissure.

Bi. Bi injection sites (cases J47FS, J52LY, and J44FR) resulted in labeled fibers in the same regions as Bpc inputs, except for the dorsomedial shell (Fig. 5). Compared to Bpc cases, Bi injection sites had additional light distributions of labeled fibers in the central rostral 'core' of the ventral striatum, and moderate to heavy labeled fibers in the ventral body of the caudate nucleus, amygdalostriatal area, ventral putamen posterior to the anterior commissure, and tail of the caudate nucleus. Anterogradely labeled fibers continued caudally to fill the genu of the caudate nucleus.

Bmc. The broad pattern of labeled fibers (cases J12FR, J16LY, and J12LY) resembled those in the Bi, including high densities of labeled fibers in the ventral body of the caudate nucleus, amygdalostriatal area, ventral putamen posterior to the anterior commissure, and tail of the caudate nucleus. Labeled fibers in the rostral ventral striatum were mainly found in the lateral shell, and Bmc injections had more labeled fibers in central domains of the caudate head compared with Bi injections.

Cortico-striatal and amygdalo-striatal paths (Cohort 2)

Injection site placement. 8 injections were placed into a range of rostral-caudal striatal regions that received amygdala input based on Cohort 1 anterograde data (Fig. 6). Of these, 6 sites had large numbers of retrogradely labeled cells in the basal nucleus, and were used for analysis. Of these, 2 injections are located in the rostral ventral striatum; J24WGA was placed in the CABP-negative dorsomedial shell, and J13WGA was placed in the CaBP-positive ventral striatal core. 4 injections are located in more caudal ventral striatal regions; J8WGA, J12WGA, and J11WGA were all placed at different levels of the caudoventral putamen. J41WGA was placed in the ventromedial body of the caudate nucleus posterior to the anterior commissure. 2 injections had relatively few labeled cells, and were not included in the analysis (J35FR and J42WGA).

Amygdala inputs delineate 'limbic' striatum regions. The basal nucleus had many labeled cells after all injections (Figs. 7A). Other amygdala nuclei, especially the accessory basal nucleus (magnocellular subdivision), had labeled cells in some cases (data not shown). In general, the total number of labeled cells in the basal nucleus was highest following rostral ventral striatal injections, decreasing with injections in progressively caudal sites (Fig 7B). With increasingly caudal injection sites, labeled cells also were found in the Bi and Bmc. The pattern of inputs from the basal nucleus subdivisions resembled the hierarchical layering of cortical inputs to the basal nucleus found in Cohort 1. The Bpc formed ubiquitous input to all striatal regions, with additional inputs sequentially added from Bi and Bmc, respectively, in increasingly caudal ventral striatal regions. We termed these caudal regions 'extended' caudal ventral striatum.

Direct cortical inputs to 'limbic' striatum regions. All 6 striatal cases contained labeled cells in both the PFC and insula (Fig. 8A). There were labeled cells in the agranular cortex after all injection sites. The injection site in the dorsomedial shell of the striatum resulted in labeled cells almost exclusively in the agranular cortices, while the injection site in the ventral striatal 'core' resulted in additional labeled cells in dysgranular cortices. Injections in more caudal sites of the ventral striatum led to more labeled cells in dysgranular and granular cortices. Overall, the greatest number of labeled cells from the PFC and insula were seen following injections into the rostral ventral striatum, with numbers tapering off following injections in more 'caudal limbic striatum'.

'Classic' ventral striatum. Agranular cortices had many labeled cells in cases J24WGA and J13WGA, particularly areas 25c, 25r, 32c, 32r, and agranular insula (Fig. 8A). Both J24WGA and J13WGA had many labeled cells specifically in areas 25 and lai, but J13WGA, placed in the ventral striatal core, had many additional labeled cells in lal, as well as many labeled cells in agranular areas 14c and 24b, and dysgranular area 13b.

Caudal ventral striatum. Injections into the caudoventral putamen (J8WGA, J11WGA, and J12WGA) and the ventral body of the caudate head (J41WGA) resulted in labeled cells in the agranular cortices, as did our rostral ventral striatal site (Fig. 8A). The number of labeled cells from agranular cortices decreased along the rostrocaudal axis overall, balanced by increasingly more labeled cells appearing in the dysgranular and granular cortices. For example, cases J8WGA and J12WGA had a majority of cell labeling in

agranular insula, but in cases J11WGA and J41WGA agranular insula labeling was more modest, with relatively more labeling in dysgranular insula. Similarly, the number of labeled neurons in agranular area 25 declined along the rostrocaudal axis. All caudal injection sites had many labeled cells in dysgranular insula, and moderate cell labeling in granular insula.

Quantitative analyses revealed hierarchical, nested projections based on basic levels of cortical differentiation (Fig. 8B). This pattern was similar to that observed in cortico-amygdala retrograde data, with agranular regions containing retrogradely labeled cells for all injection sites, and increasingly caudal regions containing labeled cells in dysgranular and granular cortices of both the insula and PFC. Analyses using a more refined (9 category) granularity classification showed similar patterns (Fig. 8-1).

Comparing granularity index for cortico-amygdala-striatal and cortico-striatal pathways. We used a 'ratio of ratios' approach to estimate how cortical granularity influenced amygdala projections to specific striatal regions in the 'indirect' pathway (see Methods) and compared these results with results for the direct pathway (Fig. 9). For all striatal injection sites, agranular cortical sources dominated in both pathways, followed by a smaller contribution from dysgranular cortices, and the smallest from granular cortices (Fig. 9A). For the indirect pathway, input from each type of cortex remained relatively stable across the rostro-caudal extent of striatal injection sites. In contrast, in the direct pathway there was a shift in the relative contribution from agranular, dysgranular, and granular cortices along the rostrocaudal axis of the amygdala-recipient

('limbic') striatum. In this path, the contribution from agranular cortical regions was progressively reduced, with increasing input from more differentiated cortices. Taken together, in the 'classic' ventral striatal regions, the balance of cortical influences is similar, whether direct, or indirectly processed through the amygdala. In more 'caudal ventral striatum', while the balance of 'indirect' cortical influence remained constant, direct inputs from the cortex varied. The agranular cortical inputs were less pronounced, but maintained a presence, along with increased dysgranular and granular cortical inputs (Fig. 9B).

Cortical granularity maps: translating to traditional cortical divisions

After analyzing data using cortical granularity criteria, we were interested in understanding how the combinations of traditional cortical regions comprised these patterns. It has long been known that 'agranular' cortices are associated with the 'limbic' system, while dysgranular cortices are considered 'paralimbic' and the most granulated cortices are associated with higher cognitive functions (Badre and D'Esposito, 2009; Barbas, 2015). Since functional studies are typically based on Brodmann's areas and atlas designations, we 'back-translated' the granularity index findings by converting the data according into its original atlas designation (Table 1)(Fig. 10).

In the cortico-amygdala path, the greatest contribution to the 'agranular' cortex was from agranular insula, where the numbers of labeled cells were greater than in all regions of the agranular cortex of the PFC combined (anterior cingulate areas 25, 24, and 32) (Fig 10A, blue). The agranular insula was associated with all basal nucleus subdivisions. In

525 the Bpc, agranular insula was surprisingly dominant compared to area 25, especially in
526 more caudomedial regions, based on cell count criteria. Labeled cells in area 25 resulted
527 mainly from injection sites in the rostro-dorsal Bpc as well as the ventral Bi. In a similar
528 manner, the number of labeled cells in areas 24 and 32 increased mainly from Bi and
529 Bmc injection sites, having little association with Bpc injection sites.
530
531 Contributions from dysgranular cortices were mainly from dysgranular area 13,
532 dysgranular area 8 (i.e. area 8B), dysgranular area 12 (i.e. 12o), and the dysgranular
533 insula (Fig. 10A, aqua, green). Area 13 was associated mostly with Bmc injection sites,
534 area 8 associated mostly with dorsal Bi and Bmc injection sites, area 12 associated mostly
535 with dorsal Bi and Bmc injection sites, and dysgranular insula associated with rostral Bpc,
536 dorsal Bi, and Bmc injection sites. In the granular cortices there was modest numbers of
537 labeled cells in regions of the dorsal and lateral PFC (areas 9, 46, 45) and frontal pole
538 (area 10). The granular insula (Ig) had the fewest labeled cells. All of these regions were
539 associated mainly with the dorsal Bi and Bmc.
540
541 In the cortico-striatal path, the agranular cortex as a whole had its largest contribution
542 from the agranular insula, followed by area 25. Labeled cells in the agranular insula were
543 associated with all striatal sites, while labeled cells in area 25 were associated mainly
544 with rostral ventral striatal injection sites. Areas 24 and 32 contained labeled cells in all
545 striatal injection sites, which were prominent in the rostral striatum, but persisted in
546 association with every caudal ventral striatal site. Contributions from the dysgranular
547 component of area 13 (i.e. area 13b) (aqua) and dysgranular insula (light green) were

548 first seen in the core of the rostral ventral striatum, and were present through the caudal
549 ventral striatum. The dysgranular insula (light green) was a key contributor following all
550 caudal ventral striatal injection sites. The number of labeled cells in combined
551 dysgranular/granular (orange/red) cortices was most prominent in area 12 (specifically
552 area 12o), with lesser contributions from other combined dysgranular/granular and fully
553 granular cortices. Labeled cells in all these regions were associated with the core of the
554 rostro-ventral striatum, and caudal ventral striatal sites. The 'core' of the rostral ventral
555 striatum had the most labeled cells overall, compared to other injection sites. Labeled
556 cells from the PFC and insula generally declined in 'extended' caudal ventral striatal
557 regions. These regions receive additional massive inputs from sensory association
558 cortices not examined in this study (Saint-Cyr et al., 1990; Yeterian and Pandya, 1995,
559 1998) (see Discussion).

560

561 ## Discussion

562 There were several important findings that emerged from these studies. The first is that
563 a ‘cortical logic’ governed by laminar structure shapes information flow in both the
564 ‘indirect’ and ‘direct’ paths to the 'limbic' striatum (Fig. 11). Agranular cortical inputs to
565 both the amygdala and striatum were foundational, undergirding inputs from incrementally
566 more differentiated cortex in a strict progression based on laminar assignment.
567 Remarkably, these basic organizational principles were also present in the amygdalo-
568 striatal path, which emanated from cytoarchitecturally defined subregions of the basal
569 nucleus. While not a laminar structure, the basal nucleus is cortical-like (Carlsen and
570 Heimer, 1988), and appears to follow hierarchical rules found in cortical projections.

571 Another key result was that the amygdala-striatal paths were influenced by a consistent
572 proportion of agranular/dysgranular/granular cortices, overwhelmingly dominated by
573 agranular cortex, regardless of whether the final target was the rostral-ventral or caudal-
574 ventral striatum. In contrast, the ratio of cortical laminar regions in the direct cortico-
575 amygdala projection was more changeable, and became gradually tipped to favor of more
576 differentiated inputs in the caudal ventral striatum.
577
578 Finally, we concluded that the 'limbic' striatum, as defined by amygdala inputs, extends
579 beyond the 'classic' ventral striatum (nucleus accumbens). Different rostrocaudal levels
580 of the 'limbic' striatum receive shifting combinations of cortical inputs, making for unique
581 'connectional fingerprints' in each region.
582
583 ***Cortical logic.*** Many individual studies have examined pathways linking cortex to
584 amygdala, amygdala to the striatum, and cortex to the striatum, using anterograde tracer
585 injections into the cortex (Mufson et al., 1981; Russchen et al., 1985; Goldman-Rakic and
586 Selemon, 1986; Carmichael and Price, 1995; Ferry et al., 2000; Ghashghaei and Barbas,
587 2002; Fudge et al., 2004). Our work builds on these studies by taking a 'connectomics'-
588 type approach, examining the relationship of multiple pathways within and across
589 animals, and assessing rules by which top-down cortex modulates down-stream targets.
590 This approach is based on a basic tenet that functional specificity is determined by
591 ensembles of afferent projections, and that the strength of any one connection depends
592 on features of the afferents that arrive with it.
593

The principles that guide the 'logic' of cortical afferents are based in the granular complexity of the cortical afferent source. The least differentiated cortical regions examined form a 'foundational' base across the basal nucleus and 'limbic' (amygdala-recipient) striatum, while inputs from more differentiated cortical regions are additive and are always seen as co-projections with these less differentiated cortical regions.

One way to view the broad 'foundational' influence of agranular cortices versus the relatively more restricted influence of differentiated cortices is by applying emerging ideas about differential functions of cortical afferent systems (Sherman and Guillery, 1998). This concept is based on Sherman and Guillery's 'driver-modulator' theory of excitatory afferents, in which a 'driver pathway' provides the main path of information flow and a co-projecting 'modulator pathway' regulates the output from 'driver' systems (Sherman and Guillery, 1998). Applied to our work here, we hypothesize that the agranular cortices of the PFC and insula are a driver system of both 'indirect' cortico-amygdala-striatal and 'direct' cortico-striatal circuits. These regions, along with the entirety of the basal nucleus and amygdala-recipient striatum form the foundational circuits that may be responsible for carrying salient emotional information forward. The other networks composed of dysgranular and granular cortices, the Bi, Bmc and caudal ventral striatum may function as modulator pathways—more restricted in their influence, with possible regulation of the foundational pathways with which they co-project. Specific anatomic and electrophysiologic properties define 'driver/modulator' paths, and can be tested in this system in the future.

617 ***"Connectivity Fingerprints" in the Basal nucleus and 'Limbic' Striatum***

618 Due to the 'logic' of cortical afferents, a predictable, yet unique set of inputs are found in
619 specific subregions of both the basal nucleus and the striatum. Unique connectivity
620 profiles ('fingerprints') are found in ventral-dorsal (basal nucleus) and rostral-caudal
621 (striatum) locations, and shift in a predictable, topographical manner.

622

623 *Basal nucleus 'fingerprints'.* Against a backdrop of broad-based agranular cortical inputs,
624 projections from increasingly dysgranular and granular cortical regions are added, and
625 overlapped in incrementally dorsal and rostral aspects of the basal nucleus. These
626 additions to connectivity appeared to closely follow differences in its pyramidal cell size
627 along the ventral (Bpc) to dorsal (Bmc) gradient of the basal nucleus. Pyramidal neurons
628 in the dorsal (Bmc) basal nucleus, which receive the most diverse set of cortical inputs,
629 are known to be the largest in the amygdala (Amaral et al., 1992), followed by decreasing
630 cell size in the intermediate and ventral basal nucleus. Cell soma size, along with synaptic
631 contact number and channel density, governs neuronal information coding (Sengupta et
632 al., 2013). Cell soma size is the factor most associated with a high information coding
633 capacity, when synaptic numbers and channel densities are held constant. Based on
634 size alone, neurons in the Bmc thus appear best-equipped for integrating the large
635 numbers of cortical afferent inputs from overlapping limbic and cognitive cortical
636 networks, as well as coordinating efferent outputs to vast striatal regions. This supports
637 our finding that the Bmc received the most diverse set of cortical inputs and projected the
638 most diverse set of striatal outputs.

639

Gradual connectional shifts in the basal nucleus may also be guided by its prenatal developmental patterns. Bmc neurons are the 'oldest' neurons in the basal nucleus based on birth-dating studies done in the fetal macaque (Kordower et al., 1992). By inference, these more dorsal basal nucleus neurons can begin the simultaneous process of somal growth and differentiation and afferentation at earlier timepoints (Purves and Lichtman, 1980; Dalva et al., 1994) , perhaps with time for contact by more diverse cortical inputs.

'Limbic' striatal 'fingerprints' The classic ventral striatum (also known as the nucleus accumbens) mediates reward-driven behaviors (Haber and Knutson, 2010) based in part on amygdala inputs (Popescu et al., 2007; Dallerac et al., 2017). In contrast, the caudal ventral striatum has long been considered important in multimodal sensory integration and discrimination, based on strong inputs from visual and auditory systems (Saint-Cyr et al., 1990; Yeterian and Pandya, 1995, 1998; Amita et al., 2019). Our data expand the connectivity profile of the caudal ventral striatum, showing it to be part of the 'limbic' striatum based on amygdala inputs. In addition to the direct agranular cortical inputs that are foundational in the entire 'limbic' striatum, the caudal ventral striatum receives additional inputs from the dysgranular insula, area 12, and area 8. These cortical regions are involved in awareness of bodily movements, and social responses (Karnath and Baier, 2010; Jezzini et al., 2012) see review (Evrard, 2019), object identification (Wilson et al., 1993), and eye and ear movement (Bon and Lucchetti, 1994), respectively. Taken together with caudal ventral striatal visual/auditory inputs in primate species, this connectional fingerprint suggests a role in motivated multisensory responses, including

663 complex social interactions involved in saccades, vocalizations, and head and neck
664 movements.
665
666 *Functional network organization.* Throughout the 'direct' and 'indirect' paths to the limbic
667 striatum, an extensive foundation is created by the agranular cortex, comprised of
668 structures involved in internal salience monitoring (Craig, 2002). This is coupled with the
669 greater specificity in dysgranular and granular cortex connectivity (regions implicated in
670 social interactions (Sliwa and Freiwald, 2017) and multi-modal sensory integration/the
671 'ventral attention network' (Fox et al., 2006), respectively). We speculate that the overlap
672 of these latter regions in paths involving the dorsal basal nucleus and caudal ventral
673 striatum may provide necessary structural organization by which social-emotional
674 behavior arises in primates. The hierarchical, layered connectivity profiles, which are
675 most expanded in these latter regions, may promote behavioral flexibility, particularly for
676 the emotional and cognitive integration required when engaging in complex social groups
677 (Chang et al., 2013).
678
679 This connectional complexity could leave the striatum, particularly the caudal striatum,
680 susceptible to neuropsychiatric diseases, particularly those in which auditory/visual
681 processing deficits interface with the limbic system. Our work shows that the caudal
682 striatum receives more 'limbic' inputs than previously noted which presumably project
683 onto, and along with, these strong visual and auditory circuit terminals (Saint-Cyr et al.,
684 1990; Yeterian and Pandya, 1995, 1998). Therefore, it is possible that abnormalities in
685 the 'connectivity fingerprint' intrinsic to the caudal striatum may be involved in perceptual

686 disturbances such as psychosis, as suggested by human neuroimaging studies (Hoffman
687 et al., 2011; Cui et al., 2016).
688
689 ***Conclusion***
690 Cortical granularity rules were elucidated in a well-known triad of connections through the
691 'limbic' brain in monkeys. Using a connectomics-type approach, we found that the basal
692 nucleus and 'limbic' striatum are not homogeneous entities, and have unique, predictable,
693 sets of 'connectivity fingerprints' within them. These general connectivity patterns have
694 implications for the ways in which the emotional brain can code increasingly complex
695 levels of social and cognitive information in a flexible manner, such as predicting actions
696 and choices of others (Saez et al., 2015; Grabenhorst et al., 2019), and may help us to
697 better understand dynamics in complex neuroanatomic circuits associated with human
698 psychiatric disease.
699
700
701
702 **Bibliography**

703 Akil H, Gordon J, Hen R, Javitch J, Mayberg H, McEwen B, Meaney MJ, Nestler EJ (2018)
704 Treatment resistant depression: A multi-scale, systems biology approach.
705 Neuroscience and biobehavioral reviews 84:272-288.
706 Amaral DG, Bassett JL (1989) Cholinergic innervation of the monkey amygdala: An
707 immunohistochemical analysis with antisera to choline acetyltransferase. J Comp
708 Neurol 281:337-361.
709 Amaral DG, Price JL, Pitkanen A, Carmichael ST (1992) Anatomical organization of the
710 primate amygdaloid complex. In: The Amygdala: Neurobiological Aspects of Emotion,
711 Memory, and Mental Dysfunction, pp 1-66: Wiley-Liss, Inc.
712 Amita H, Kim HF, Smith MK, Gopal A, Hikosaka O (2019) Neuronal connections of direct and
713 indirect pathways for stable value memory in caudal basal ganglia. The European
714 journal of neuroscience 49:712-725.

715 Badre D, D'Esposito M (2009) Is the rostro-caudal axis of the frontal lobe hierarchical?
716 Nature reviews Neuroscience 10:659-669.
717 Barbas H (2007) Specialized elements of orbitofrontal cortex in primates. Annals of the New
718 York Academy of Sciences 1121:10-32.
719 Barbas H (2015) General cortical and special prefrontal connections: principles from
720 structure to function. Annual review of neuroscience 38:269-289.
721 Barbas H, Pandya DN (1989) Architecture and intrinsic connections of the prefrontal cortex
722 in the rhesus monkey. J Comp Neurol 286:353-375.
723 Barbas H, Garcia-Cabezas MA (2016) How the prefrontal executive got its stripes. Curr Opin
724 Neurobiol 40:125-134.
725 Bon L, Lucchetti C (1994) Ear and eye representation in the frontal cortex, area 8b, of the
726 macaque monkey: an electrophysiological study. Exp Brain Res 102:259-271.
727 Braak H, Braak E (1983) Neuronal types in the basolateral amygdaloid nuclei of man. Brain
728 research bulletin 11:349-365.
729 Brodmann K (1909) "Vergleichende Lokalisationslehre der Grosshirnrinde" (Comparitive
730 Localization Theory of the Cerebral Cortex: Illustrated in its Principles on the Basis of
731 Cell Construction). Leipzig: J.A. Barth.
732 Carlsen J, Heimer L (1988) The basolateral amygdaloid complex as a cortical-like structure.
733 Brain research 441:377-380.
734 Carmichael ST, Price JL (1994) Architectonic subdivision of the orbital and medial prefrontal
735 cortex in the macaque monkey. J Comp Neurol 346:366-402.
736 Carmichael ST, Price JL (1995) Limbic connections of the orbital and medial prefrontal cortex
737 in macaque monkeys. J Comp Neurol 363:615-641.
738 Chang SW, Brent LJ, Adams GK, Klein JT, Pearson JM, Watson KK, Platt ML (2013)
739 Neuroethology of primate social behavior. Proceedings of the National Academy of
740 Sciences of the United States of America 110 Suppl 2:10387-10394.
741 Cho YT, Ernst M, Fudge JL (2013) Cortico-Amygdala-Striatal Circuits Are Organized as
742 Hierarchical Subsystems through the Primate Amygdala. The Journal of neuroscience
743 : the official journal of the Society for Neuroscience 33:14017-14030.
744 Craig AD (2002) How do you feel? Interoception: the sense of the physiological condition of
745 the body. Nature Reviews Neuroscience 3:655-666.
746 Cui LB, Liu K, Li C, Wang LX, Guo F, Tian P, Wu YJ, Guo L, Liu WM, Xi YB, Wang HN, Yin H
747 (2016) Putamen-related regional and network functional deficits in first-episode
748 schizophrenia with auditory verbal hallucinations. Schizophr Res 173:13-22.
749 Dallerac G, Graupner M, Knippenberg J, Martinez RC, Tavares TF, Tallot L, El Massioui N,
750 Verschueren A, Hohn S, Bertolus JB, Reyes A, LeDoux JE, Schafe GE, Diaz-Mataix L,
751 Doyere V (2017) Updating temporal expectancy of an aversive event engages striatal
752 plasticity under amygdala control. Nature communications 8:13920.
753 Dalva MB, Ghosh A, Shatz CJ (1994) Independent control of dendritic and axonal form in the
754 developing lateral geniculate nucleus. The Journal of neuroscience : the official
755 journal of the Society for Neuroscience 14:3588-3602.
756 Decampo DM, Fudge JL (2013) Amygdala projections to the lateral bed nucleus of the stria
757 terminalis in the macaque: Comparison with ventral striatal afferents. The Journal of
758 comparative neurology 521:3191-3216.
759 Evrard HC (2019) The Organization of the Primate Insular Cortex. Front Neuroanat 13:43.

760 Ferry AT, Ongur D, An X, Price JL (2000) Prefrontal cortical projections to the striatum in
761 macaque monkeys: evidence for an organization related to prefrontal networks.
762 Journal of Comparative Neurology 425:447-470.
763 Fox MD, Corbetta M, Snyder AZ, Vincent JL, Raichle ME (2006) Spontaneous neuronal activity
764 distinguishes human dorsal and ventral attention systems. Proceedings of the
765 National Academy of Sciences of the United States of America 103:10046-10051.
766 Fudge JL, Haber SN (2002) Defining the caudoventral striatum in primates: cytoarchitectural
767 and histochemical features. Journal of Neuroscience 22:10078-10082.
768 Fudge JL, Breitbart MA, McClain C (2004) Amygdaloid inputs define a caudal component of
769 the ventral striatum in primates. Journal of Comparative Neurology 476:330-347.
770 Fudge JL, deCampo DM, Becoats KT (2012) Revisiting the hippocampal-amygdala pathway
771 in primates: association with immature-appearing neurons. Neuroscience 212:104-
772 119.
773 Fudge JL, Breitbart MA, Danish M, Pannoni V (2005) Insular and gustatory inputs to the
774 caudal ventral striatum in primates. The Journal of comparative neurology 490:101-
775 118.
776 Fudge JL, Kunishio K, Walsh P, Richard C, Haber SN (2002) Amygdaloid projections to
777 ventromedial striatal subterritories in the primate. Neuroscience 110:257-275.
778 Geneser-Jensen FA, Blackstad TW (1971) Distribution of acetyl cholinesterase in the
779 hippocampal region of the guinea pig. Z Zellforsch 114:460-481.
780 Ghashghaei HT, Barbas H (2002) Pathways for emotion: interactions of prefrontal and
781 anterior temporal pathways in the amygdala of the rhesus monkey. Neuroscience
782 115:1261-1279.
783 Goldman-Rakic PS, Selemon LD (1986) Topography of corticostriatal projections in
784 nonhuman primates and implications for functional parcellation of the neostriatum.
785 In: Cerebral Cortex Vol. 5 (Jones EG, Peters A, eds), pp 447-466. New York: Plenum
786 Publishing Corporation.
787 Grabenhorst F, Baez-Mendoza R, Genest W, Deco G, Schultz W (2019) Primate Amygdala
788 Neurons Simulate Decision Processes of Social Partners. Cell 177:986-998 e915.
789 Gu Z, Gu L, Eils R, Schlesner M, Brors B (2014) circlize Implements and enhances circular
790 visualization in R. Bioinformatics 30:2811-2812.
791 Haber SN, Knutson B (2010) The reward circuit: linking primate anatomy and human
792 imaging. Neuropsychopharmacology : official publication of the American College of
793 Neuropsychopharmacology 35:4-26.
794 Haber SN, Fudge JL, McFarland N (2000) Striatonigrostriatal pathways in primates form an
795 ascending spiral from the shell to the dorsolateral striatum. Journal of Neuroscience
796 20(6):2369-2382.
797 Herzog AG, Van Hoesen GW (1976) Temporal neocortical afferent connections to the
798 amygdala in the rhesus monkey. Brain Res 115:57-69.
799 Hoffman RE, Fernandez T, Pittman B, Hampson M (2011) Elevated functional connectivity
800 along a corticostriatal loop and the mechanism of auditory/verbal hallucinations in
801 patients with schizophrenia. Biological psychiatry 69:407-414.
802 Jezzini A, Caruana F, Stoianov I, Gallese V, Rizzolatti G (2012) Functional organization of the
803 insula and inner perisylvian regions. Proceedings of the National Academy of Sciences
804 of the United States of America 109:10077-10082.

Karnath HO, Baier B (2010) Right insula for our sense of limb ownership and self-awareness of actions. Brain structure & function 214:411-417.

Klavir O, Genud-Gabai R, Paz R (2013) Functional connectivity between amygdala and cingulate cortex for adaptive aversive learning. Neuron 80:1290-1300.

Kordower JH, Piecinski P, Rakic P (1992) Neurogenesis of the amygdaloid nuclear complex in the rhesus monkey. Brain research Developmental brain research 68:9-15.

Likhtik E, Stujenske JM, Topiwala MA, Harris AZ, Gordon JA (2014) Prefrontal entrainment of amygdala activity signals safety in learned fear and innate anxiety. Nature neuroscience 17:106-113.

Meredith GE, Pattiselanno A, Groenewegen HJ, Haber SN (1993) Shell and core in the primate ventral striatum identified with antibodies against calbindin. Soc Neurosci Abst.

Mesulam M-M, Mufson EJ (1982) Insula of the Old World Monkey. I: Architectonics in the insulo-orbito-temporal component of the paralimbic brain. J Comp Neurol 212:1-22.

Mufson EJ, Mesulam MM, Pandya DN (1981) Insular interconnections with the amygdala in the rhesus monkey. Neuroscience 6:1231-1248.

Nieuwenhuys R, Voogd J, Huijzen CV (2007) Th Human Central Nervous System: A Synopsis and Atlas, 4 Edition: Springer.

Petrides M, Pandya DN (1999) Dorsolateral prefrontal cortex: comparative cytoarchitectonic analysis in the human and the macaque brain and corticocortical connection patterns. European Journal of Neuroscience 11:1011-1036.

Petrides M, Pandya DN (2002) Comparative cytoarchitectonic analysis of the human and the macaque ventrolateral prefrontal cortex and corticocortical connection patterns in the monkey. The European journal of neuroscience 16:291-310.

Popescu AT, Saghyan AA, Pare D (2007) NMDA-dependent facilitation of corticostriatal plasticity by the amygdala. Proceedings of the National Academy of Sciences of the United States of America 104:341-346.

Popescu AT, Popa D, Pare D (2009) Coherent gamma oscillations couple the amygdala and striatum during learning. Nature neuroscience.

Preuss TM, Goldman-Rakic PS (1991) Myelo-and cytoarchitecture of the granular frontal cortex and surrounding regions in the strepsirhine primate galago and the anthropoid primate macaca. J Comp Neurol 310:429-474.

Purves D, Lichtman JW (1980) Elimination of synapses in the developing nervous system. Science 210:153-157.

Ressler KJ (2020) Translating Across Circuits and Genetics Toward Progress in Fear- and Anxiety-Related Disorders. The American journal of psychiatry 177:214-222.

Robbins TW, Cador M, Taylor JR, Everitt BJ (1989) Limbic-striatal interactions in reward-related processes. Neuroscience & Biobehavioral Reviews 13:155-162.

Rose M (1928) Die inselrinde des menschen und der tiere. J Psychol Neurol 37:467-624.

Rosene DL, Roy NJ, Davis BJ (1986) A cryoprotection method that facilitates cutting frozen sections of whole monkey brains for histological and histochemical processing without freezing artifact. J Histochem Cytochem Vol. 34, No. 10:1301-1315.

Russchen FT, Bakst I, Amaral DG, Price JL (1985) The amygdalostriatal projections in the monkey. An anterograde tracing study. Brain Res 329:241-257.

Saez A, Rigotti M, Ostojic S, Fusi S, Salzman CD (2015) Abstract Context Representations in Primate Amygdala and Prefrontal Cortex. Neuron 87:869-881.

Saint-Cyr JA, Ungerleider LG, Desimone R (1990) Organization of visual cortical inputs to the striatum and subsequent outputs to the pallido-nigral complex in the monkey. J Comp Neurol 298:129-156.

Saunders RC, Rosene DL, Van Hoesen GW (1988) Comparison of the efferents of the amygdala and the hippocampal formation in the rhesus monkey: II. Reciprocal and non-reciprocal connections. J Comp Neurol 271:185-207.

Sengupta B, Faisal AA, Laughlin SB, Niven JE (2013) The effect of cell size and channel density on neuronal information encoding and energy efficiency. J Cereb Blood Flow Metab 33:1465-1473.

Sherman SM, Guillery RW (1998) On the actions that one nerve cell can have on another: Distinguishing "drivers" from "modulators". Proceedings of the National Academy of Sciences of the United States of America 95:7121-7126.

Sliwa J, Freiwald WA (2017) A dedicated network for social interaction processing in the primate brain. Science 356:745-749.

Stephan H, Frahm HD, Baron G (1987) Comparison of brain structure volumes in insectivora and primates VII. Amygdaloid components. J Hirnforsch 5:571-584.

Van Hoesen GW, Yeterian EH, Lavizzo-Mourney R (1981) Widespread corticostriate projections from temporal cortex of the rhesus monkey. J Comp Neurol 1981:205-219.

Walker AE (1940) A cytoarchitectural study of the prefronal area of the macaque monkey. J Comp Neurol 73:59-86.

Wilson FA, Scalaidhe SP, Goldman-Rakic PS (1993) Dissociation of object and spatial processing domains in primate prefrontal cortex. Science 260:1955-1958.

Yeterian EH, Pandya DN (1995) Corticostriatal connections of extrastriate visual areas in rhesus monkeys. Journal of Comparative Neurology 352:436-457.

Yeterian EH, Pandya DN (1998) Corticostriatal connections of the superior temporal region in rhesus monkeys. Journal of Comparative Neurology 399:384-402.

Yeterian EH, Pandya DN, Tomaiuolo F, Petrides M (2012) The cortical connectivity of the prefrontal cortex in the monkey brain. Cortex 48:58-81.

Figure legends

Figure 1: Study design. Cohort 1 animals (bi-directional tracer studies, purple) had a series of injections placed in different subdivisions of the basal nucleus of the amygdala. Resulting retrogradely labeled cells in the PFC and Insula were quantified; anterogradely labeled fibers in the striatum were mapped to guide injections in Cohort 2. Cohort 2 animals (retrograde studies, orange) had a series of injections placed in different regions of the striatum that were 'amygdala-recipient' (i.e. striatal regions with labeled fibers in Cohort 1 animals). Retrogradely labeled cells in the amygdala, and the PFC and Insula, were quantified.

888

889 **Figure 2:** Relative levels of cortical lamination in the PFC and Insula in the Macaque. ***A***. Ventral
890 view ***B***. Sagittal view from the midline ***C***. Lateral view, with lateral fissure 'opened' for ***C'.*** view of
891 insula. Image adapted from Carmichael & Price, 1994 and Saleem & Price, 2008. The key
892 illustrates the range of cortical differentiation; shades of blue indicate agranular cortex, shades of
893 green indicate dysgranular cortex, and shades of red indicate granular cortex. The darker the
894 shade within each granularity grouping indicates increased development of layer IV, layer II,
895 and/or layer V of cortex. Insets are from cresyl violet stained sections that give examples of
896 laminar regions in agranular, dysgranular and granular cortices. Bar = 500 um.
897 *Abbreviations: 6, area 6 (premotor/supplementary motor area); 8Ad, dorsal area 8A; 8Av,*
898 *ventral area 8A; 8B, area 8B; 9, area 9; 9m, medial area 9; 9/46d, dorsal area 9/46; 9/46v,*
899 *ventral area 9/46; 10m, medial area 10; 10o, orbital area 10; 11l, lateral area 11; 11m, medial*
900 *area 11; 12l, lateral area 12; 12m, medial area 12; 12o, orbital area 12; 12r, rostral area 12;*
901 *13a, area 13a; 13b, area 13b; 13l, lateral area 13; 13m, medial area 13; 14c, caudal area 14;*
902 *14r, rostral area 14; 24a, area 24a; 24b, area 24b; 24c, area 24c; 25c, caudal area 25; 25r,*
903 *rostral area 25; 32c, caudal area 32; 32r, rostral area 32, 45, area 45; 46, area 46; 9/46d,*
904 *dorsal area 9/46; area 9/46v, ventral area 9/46; cc, corpus callosum; G, gustatory cortex; Iai,*
905 *intermediate agranular insula area; Ial, lateral agranular insula area; Iam, medial agranular*
906 *insula area; Iapl, posterolateral agranular insula area; Iapm, posteromedial agranular insula*
907 *area; Id, dysgranular insula; Ig, granular insula; ob, olfactory bulb; oc, optic chiasm; PrCO,*
908 *precentral opercular area.*

909

910 **Table 1:** Laminar characteristics of the PFC and insula subdivisions, and 3- and 9-group
911 granularity assignments. Each column indicates the main granularity grouping of every
912 Brodmann's area examined (i.e. the relative thickness of layer IV of cortex). The darker the

913 shade within each sub-section within each column (i.e. 'Agranular 1' vs. 'Agranular 2') represents
914 the increasing degree of layer V sublamination and/or layer IV development within each
915 granularity assignment.
916
917 **Figure 3:** Schematic of injection site locations in basal nucleus. ***A***. Injection site locations (gray)
918 in rostro-central Bmc, Bi, and Bpc. ***B***. Injection site locations (gray) in caudal Bpc. ***C***. Dark-field
919 photomicrograph of injection site location for J16LY, indicated with a white arrow. ***D***. Adjacent
920 AChE-stained section matched to ***C.*** to localize injection to basal nucleus subdivision (Bmc). ***E***.
921 Dark-field photomicrograph of the injection site location for J47FS, indicated with a white arrow.
922 ***F***. Adjacent AChE-stained section matched to ***E.*** to localize injection site within basal nucleus
923 subdivision (Bi). ***G.*** Dark-field photomicrograph of the injection site location for J15FS, indicated
924 with a white arrow. ***H.*** Adjacent AChE-stained section matched to ***H.*** to localize injection site
925 within basal nucleus subdivision (Bpc). Photos taken at 2x magnification. Scale bars = 500 μm.
926 *Abbreviations: AB, accessory basal nucleus; Bi, intermediate basal nucleus; Bmc, magnocellular*
927 *basal nucleus; Bpc, parvicellular basal nucleus; L, lateral nucleus; P, putamen; V, ventricle.*
928
929 **Figure 4:** Cortico-amygdala path. ***A.*** Representative charts showing the pattern of retrogradely
930 labeled cells in the PFC and insula resulting from 6 non-overlapping injection sites along the
931 dorsal-ventral extent of the basal nucleus. ***a'.*** The photomicrograph inset shows an example of
932 densely concentrated retrogradely labeled cells in the lal of J15FS. Scale bar = 100 μm ***B.***
933 Chord diagram showing quantitative analysis of all retrogradely labeled cells (1:24 sections)
934 through PFC and insula, classified by laminar differentiation. The top axis of this diagram shows
935 the total number of labeled cells in agranular (blue), dysgranular (green), and granular (red)
936 cortical areas across all cases examined. The bottom axis shows the number of labeled cells in
937 agranular, dysgranular, and granular cortices resulting from each basal nucleus injection site.

938 Injection sites are arranged counter-clockwise from the most caudal-ventral (left) to most rostral-
939 dorsal injection site location (right). 1 tick mark= 180 cells.
940 *Abbreviations: AC, anterior commissure; C, caudate; cc, corpus callosum; IC, internal capsule;*
941 *oc, optic chiasm; NA, nucleus accumbens; P, putamen, V, ventricle. For cortical abbreviations,*
942 *see "Abbreviations" in Figure 2 legend.*
943
944 **Extended Figure 4-1:** Cortico-amygdala chord diagram showing additional quantitative analysis
945 of retrograde labeling using 9-group granularity analysis. The top axis shows the total number of
946 labeled cells in agranular (3 shades of blue), dysgranular (3 shades of green), and granular (3
947 shades of red) cortical areas across all cases examined. The darker the shade within each
948 granularity grouping indicates increased development of layer IV, layer II, and/or layer V of
949 cortex. The bottom axis of this diagram shows the number of labeled cells from each granularity
950 subgroup that results from each basal nucleus injection site. The bottom axis is organized
951 counter-clockwise by most caudal-ventral (left) to most rostral-dorsal (right) injection site
952 location. Each tic mark for both the top and bottom axes represents 180 cells.
953
954 **Figure 5:** Representative charts showing distribution of anterogradely labeled fibers resulting
955 from the same 6 non-overlapping injection sites shown in Fig. 4, along the dorsal-ventral extent
956 of the basal nucleus. Injection sites arranged from caudo-medial (Bpc) to rostro-dorsal (Bmc)
957 across the top. Striatal section are organized from rostral to caudal levels under each injection
958 site. Photomicrograph inset shows high density patch of labeled fibers in the caudal ventral
959 putamen (darkfield). Bar = 500 μm.
960 *Abbreviations: AC, anterior commissure; C, caudate; C(g), genu of the caudate nucleus; C(t),*
961 *tail of the caudate nucleus; GP, globus pallidus; GPe; external globus pallidus; GPi, internal*
962 *globus pallidus; IC, internal capsule; lAstr, lateral amygdalostriatal area; LGN, lateral geniculate*

963 *nucleus; IIPAC, lateral interstitial nucleus of the posterior limb of the anterior commissure; mAstr,*
964 *medial amygdalostriatal area; mIPAC, medial interstitial nucleus of the posterior limb of the*
965 *anterior commissure; OT, optic tract; P, putamen; V, ventricle.*
966
967 **Figure 6:** Striatal Injection sites in Cohort 2. ***A. - D.*** Schematics of retrograde injection site
968 locations from the rostral (A) to progressively caudal regions (B-D). Medium gray sites (solid
969 lines) depict injections with significant labeled cells in amygdala, included for analysis; light gray
970 sites (dotted lines) resulted in few labeled cells in the amygdala. ***E-F.*** Brightfield
971 photomicrographs in the classic ventral striatum. ***E***. Injection site location in dorsomedial shell,
972 with adjacent CaBP-stained section (***E'.***) showing injection alignment in CaBP-negative shell**.** ***F.***
973 Injection site in the rostral 'core', with adjacent CaBP-stained section (**F'**.) showing shell/core
974 boundary. ***G-J****.* Caudal 'limbic' striatum injection sites. ***G.*** caudoventral putamen at the level of
975 the anterior commissure, ***H.*** caudoventral putamen posterior to the anterior commissure. ***I.***
976 ventral body of caudate nucleus **.** ***J.*** Injection site location in caudomedial putamen at the level
977 of the hippocampus. Scale bars = 1mm.
978 *Abbreviations: AC, anterior commissure; C, caudate; Co, ventral striatum core; GPe; external*
979 *globus pallidus; GPi, internal globus pallidus; IC, internal capsule; P, putamen; Sh, ventral*
980 *striatum shell.*
981
982 **Figure 7:** Amygdalo-striatal path. ***A.*** Charts of retrogradely labeled cells through the
983 rostrocaudal basal nucleus following injections in Cohort 2. Injection sites arranged from rostral
984 (top) to caudal (bottom). All 6 cases resulted in many retrogradely labeled cells in the basal
985 nucleus. Cell labeling in other nuclei (shaded in gray) is not shown for clarity. ***B.*** Chord diagram
986 showing numbers of labeled cells in the Bpc, Bi, and Bpc by injection site placement. The top
987 axis of this diagram shows the total number of labeled cells in Bpc (cyan), Bi (fuchsia), and Bmc
988 (purple) across all cases examined. The bottom axis shows the number of labeled cells in each

basal nucleus subdivision resulting from each striatal injection site, and is arranged counter-clockwise from the most rostral (left) to most caudal (right) injection site location. Each tick mark for both the top and bottom axes = 60 cells.

Figure 8: Cortico-'limbic' striatal path. ***A.*** Representative charts depicting retrogradely labeled cells in the PFC and insula after injections in various striatal regions along the rostral-caudal extent of the 'limbic' striatum. Cases J24WGA and J13WGA had injections in shell and core of the 'classic' ventral striatum, respectively. Injection sites in J8WGA, J12WGA, J41WGA, and J11WGA were placed in different parts of the 'extended' ventral striatum. ***B.*** Chord diagram showing the number of retrogradely labeled cells in agranular (blue), dysgranular (green), and granular (red) cortical areas across all cases examined (top axis). The bottom axis shows the number of labeled cells found in agranular, dysgranular, and granular cortices after each striatal injection site. The bottom axis is arranged counter-clockwise from the most rostral (left) to the most caudal (right) injection site location. Each tick mark represents 400 cells.

Figure 8-1 : Cortico-striatal chord diagram showing additional quantitative analysis of retrograde labeling using 9-group granularity analysis. The top axis of this diagram follows the same color schema as described in **Figure 4-1.** The bottom axis of this diagram shows the number of labeled cells from each granularity subgrouping that results from each striatal injection site. The bottom axis is organized counter-clockwise by most rostral (left) to most caudal (right) injection site location. Each tic mark for both the top and bottom axes represents 400 cells.

Figure 9: Indirect and direct pathway analysis**.** ***A.*** Composite diverging bar plots of each striatal injection showing the proportion of labeled cells in agranular (blue), dysgranular (green) and granular (red) cortices after calculating indirect pathway and direct pathway labeled cells. The

proportion of labeled cells associated with amygdala inputs to all striatal sites ('indirect' path) is relatively consistent with a large percentage of cells categorized as agranular, and consistently small percentages of labeled cells categorized as dysgranular and granular, respectively. In contrast, the 'direct' cortico-'limbic' striatal path shows more variation with rostral ventral striatal sites having the greatest proportion of labeled cells in agranular cortices, and relatively small contributions from the dysgranular and granular cortices. This balance shifts at progressively caudal ventral levels, with reductions in labeled cells in agranular cortices, and incrementally more labeled cells in dysgranular cortices > granular cortices. ***B.*** Individual cases plotted for each path.

Figure 10: Brodmann's classification. ***A.*** Additional quantitative analysis of retrograde cortico-amygdala cell labeling using Brodmann's classification. The top axis of this diagram shows the total number of labeled cells in Brodmann's areas examined. Blue indicates this Brodmann's area is exclusively agranular cortex, blue-green indicates this Brodmann's area contains a mix of agranular and dysgranular cortex, green indicates this Brodmann's area is exclusively dysgranular cortex, orange indicates this Brodmann's area contains a mix of dysgranular and granular cortex, and red indicates this Brodmann's area is exclusively granular cortex. The bottom axis of this diagram shows the number of labeled cells from each Brodmann's area that results from each basal nucleus injection site. The bottom axis is organized counter-clockwise by most caudal-ventral (left) to most rostral-dorsal injection (right) injection site location. Each tic mark for both the top and bottom axes represents 180 cells. ***B.*** Additional quantitative analysis of retrograde cortico-striatal cell labeling using Brodmann's classification, indicated on the top axis. The same color schema describe in ***A.*** applies here. The bottom axis of this diagram shows the number of labeled cells from each granularity subgrouping that results from each striatal injection site. The bottom axis is organized counter-clockwise by most rostral (left) to most caudal (right) injection site location. Each tic mark for both the top and bottom axes represents 400

cells.

Figure 11: Overview of 'cortical logic' in the 'indirect' pathway (PFC/Insula → amygdala connectivity, left + amygdala → 'limbic' striatum connectivity , bottom) and the 'direct' pathway (PFC/Insula → 'limbic' striatum connectivity, right).

Supplemental Methods

Brodmann's areas (Fig. 2)

Ventromedial Prefrontal cortex (vmPFC) and dmPFC. The medial prefrontal cortex (mPFC) is comprised of the medial frontopolar cortices, the cortex of the superior frontal gyrus, anterior cingulate, and the gyrus rectus, which gradually transition from granular cortex in the frontal poles to agranular cortex in the ventral anterior cingulate. Behind the frontopolar mPFC (granular area 10m), the dmPFC contains medial aspects of dysgranular areas 9 and 8B, which continue onto the lateral convexity (Figs. 2A & 2B) (Walker, 1940; Preuss and Goldman-Rakic, 1991; Petrides and Pandya, 1999). These regions are dorsal to the anterior cingulate cortex. The cingulate cortex, which includes areas 24a-c, 32, and 25, are all agranular. Out of these areas, ventral area 25 is the least differentiated (Carmichael and Price, 1994; Nieuwenhuys et al., 2007). Areas 32 and 24 are relatively more differentiated rostrally and dorsally, respectively. Similarly, area 14 granularity changes through its rostral-caudal extent. Area 14r is dysgranular cortex, while areas 14c is agranular cortex (Carmichael and Price, 1994).

OFC. The OFC houses one agranular subdivision (area 13a), but is largely composed of dysgranular and granular subdivisions (Fig. 2C). The most rostral extent of OFC is

1062 composed of dysgranular area 12r and granular areas 10o (frontal pole), 11m, and 11l.
1063 Posterior to these regions are granular area 12m and dysgranular areas 13b, 13m, and
1064 13l. The most posterior reaches of the OFC, which form a continuum with the insula, are
1065 dysgranular area 12o and agranular area 13a.
1066
1067 *vlPFC and dlPFC.* The vlPFC is composed of areas 45 and 12l (Walker, 1940; Preuss
1068 and Goldman-Rakic, 1991; Carmichael and Price, 1994; Petrides and Pandya, 2002)
1069 (Figs. 2A and 2C). Both areas 45 and 12l are granular, but area 45 is more differentiated
1070 than area 12l. The dlPFC is composed of areas 8B, 8Ad, 8Av, 9, 9/46d, 9/46v, and 46
1071 (Figs. 2A and 2B), and is contiguous with the underlying vlPFC (Fig. 2B). It is considered
1072 isocortex, but it also contains a gradient of differentiation. Area 8B is mostly contained in
1073 the dlPFC, but also descends into the medial wall (Fig. 2A). Area 8B and area 9 have a
1074 poorly distinguished layer IV, and are the only dysgranular areas within the
1075 overwhelmingly granular dlPFC (Preuss and Goldman-Rakic, 1991; Petrides and
1076 Pandya, 1999); The other regions of the dlPFC (areas 46, 9/46, and 8A) are granular
1077 cortex. Area 46 is found in the rostral-most extent of the sulcus principalis. Area 9/46 is
1078 more caudal than area 46, and is divided into a dorsal (9/46d) and a ventral (9/46v)
1079 component based on its relative position along the sulcus principalis. Areas 8Ad and 8Av
1080 are generally more caudal (and lateral) than areas 46, 9/46d, & 9/46v, have a broad and
1081 densely packed layer IV, and are the most highly differentiated PFC regions.
1082
1083 *Insula.* The anterior insula forms a continuum with the OFC, and resides on the caudal
1084 orbital surface (Rose, 1928; Carmichael and Price, 1994; Nieuwenhuys et al., 2007) (also

known as ‘proisocortex’ in other studies (Barbas and Pandya, 1989)). Here, the agranular insula is composed of several subdivisions, with the most undifferentiated being the posteromedial insula (Iapm) and anterior medial insula (Iam), with slightly more differentiated agranular regions (the intermediate insula (Iai), lateral insula (Ial), and posterolateral agranular insula (Iapl)) found most laterally (Carmichael and Price, 1994) (Figs. 2C & 2D). Progressing into the bank of the Sylvian fissure, the ventral insula is agranular, with progressively more differentiated insula found dorsally (Fig. 2D).

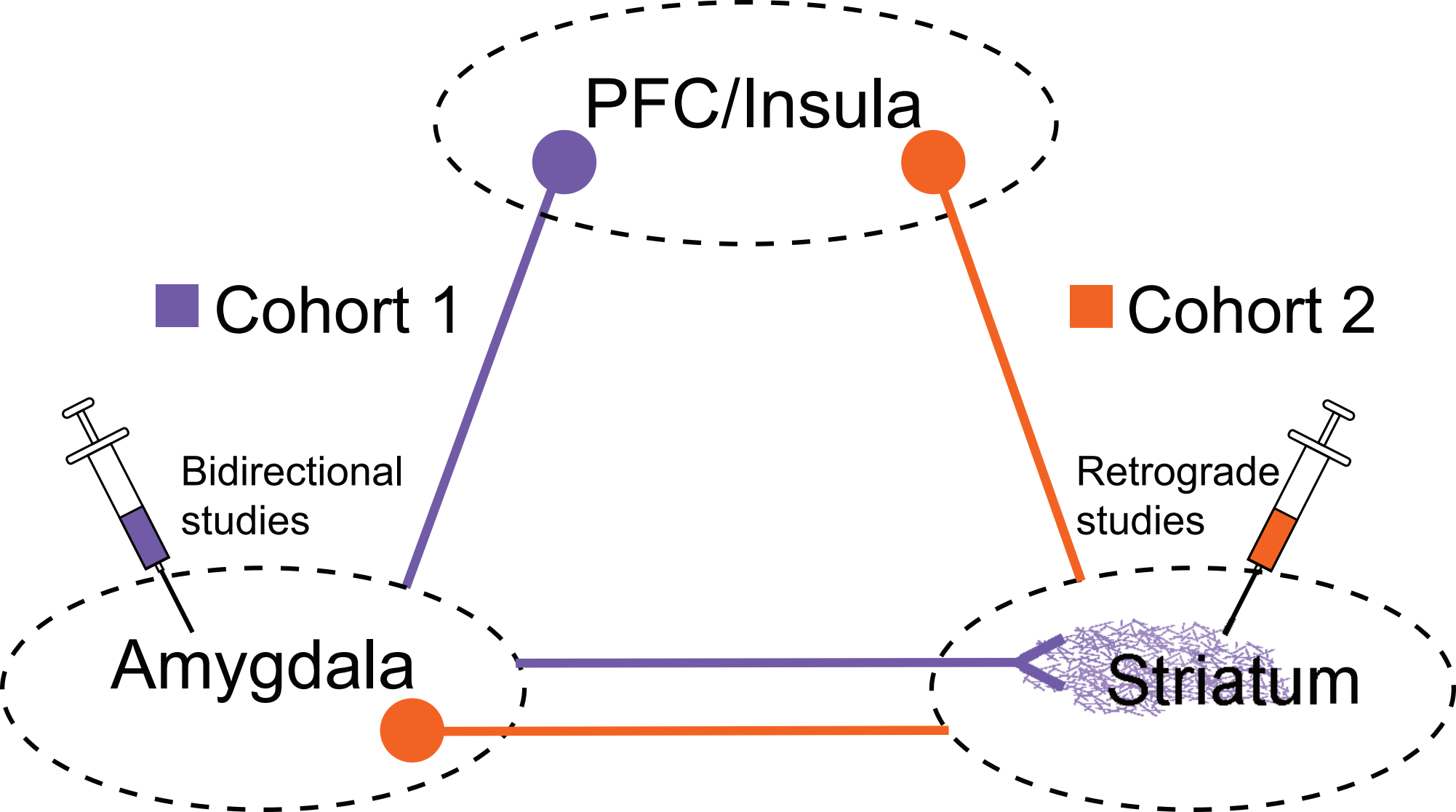
PFC/Insula
Cohort 1
Cohort 2
Bidirectional
studies
Retrograde
studies
Amygdala
Striatum

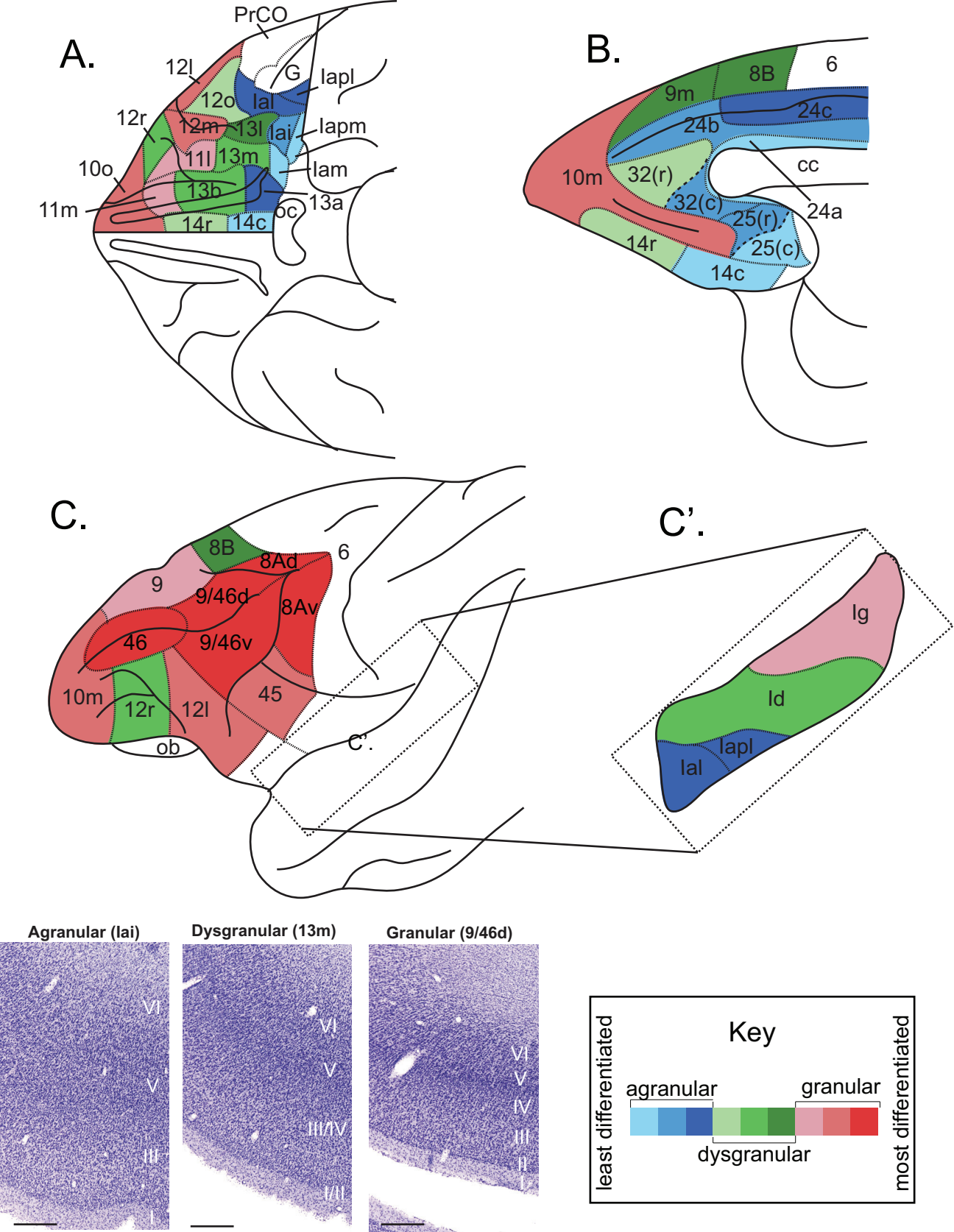
A.
PrCO
12l
G
lapl
12o
lal
12r
12m
13l
lal
lapm
11l
13m
10o
lam
13b
11m
13a
14r
14c
oc
B.
8B
6
9m
24c
24b
cc
10m
32(r)
32(c)
25(r)
24a
14r
25(c)
14c
C.
8B
8Ad
6
9
9/46d
8Av
46
9/46v
10m
12r
12l
45
ob
C'.
C'.
lg
ld
lapl
lal
Agranular (lai)
Dysgranular (13m)
Granular (9/46d)
VI
V
III
I
VI
V
III/IV
I/II
VI
V
IV
III
II
I
Key
agranular
granular
dysgranular
least differentiated
most differentiated

Table 1: Rationale for 3- and 9-group granularity assignments

Agranular	
Granularity Grouping	Reason for granularity grouping
Agranular 1	
Iam	No layer IV, and no layer V sublamination. (Carmichael & Price, 1994)
Iapm	No layer IV, and no layer V sublamination. (Carmichael & Price, 1994)
25c	No layer IV, less developed compared to 32c, 32r, and 25r. (Carmichael & Price, 1994)
24a	Has only 4 cortical layers and rudimentary lamination. (Carmichael & Price, 1994)
14c	Has only 4 cortical layers. (Carmichael & Price, 1994)
Agranular 2	
32c	No layer IV; Caudal 32 resembles 25r; has horizontal striations of pyramidal cells in layer V. (Carmichael & Price, 1994)
25r	No layer IV; caudal 32 resembles 25r. (Carmichael & Price, 1994)
24b	No layer IV; has more prominent vertical striations in layer V compared to 24c. (Carmichael & Price, 1994)
Iai	No layer IV; has partially sublaminated layer V; superficial layer V has row of large pyramidal cells. (Carmichael & Price, 1994)
Agranular 3	
Ial	No layer IV; layer V is sublaminated. (Carmichael & Price, 1994)
Iapl	No layer IV; layer V is sublaminated. (Carmichael & Price, 1994)
13a	No layer IV; layer V is sublaminated. (Carmichael & Price, 1994)
24c	No layer IV; Has pyramidal cell aggregates in layer V. (Carmichael & Price, 1994)

Dysgranular	
Granularity Grouping	Reason for granularity grouping
Dysgranular 1	
32r	Is more developed than 32c and 25r and is slightly dysgranular (Carmichael & Price, 1994). No layer V sublamination.
12o	Very weakly staining layer IV, no layer V sublamination. (Carmichael & Price, 1994)
14r	Has distinct small cells in layer II, no horizontal or vertical striations in layer V. (Carmichael & Price, 1994)
Dysgranular 2	
13b	Has horizontal and vertical striations in layer V. (Carmichael & Price, 1994)
12r	Has vertical striations in layer V, but it is not sublaminated. (Carmichael & Price, 1994)
13m	Has a sparse granular layer. Has no/less distinct sublamination of layer V (and layer III). (Carmichael & Price, 1994)
Id	Has thin layer IV with clusters of granular cells interrupted by pyramidal cells. No layer II. Almost identical in appearance to dysgranular component of caudal OFC. (Mesulam & Mufson, 1982)
Dysgranular 3	
13l	Has poorly developed layer IV and has clearly sublaminated layer V. (Carmichael & Price, 1994)
8B	Layer II is well defined; Layer IV is poorly developed and layer V blends with layer VI, but layer V is sublaminated (it has a few darkly stained cells in layer Va). (Petrides & Pandya, 1999)
9m	Has a more narrow and cell sparse layer IV than 9. (Petrides & Pandya, 1999)

Granular	
Granularity Grouping	Reason for granularity grouping
Granular 1	
9	Has a narrow layer IV. Layer Va has deeply pigmented cells and layer Vb blends with layer VI. (Petrides & Pandya, 1999)
Ig	Layer II has moderately advanced granularity, and layer IV has prominent granularity. Layer V and VI are not fully differentiated from each other; (Layer III is bilaminate).(Mesulam & Mufson, 1982)
11m	Granular with bilaminate layer V. Layer V is thinner and more trilaminate than in 13m. Outer and inner sublaminae are broken into aggregates of neurons. (Carmichael & Price, 1994)
11l	Granular with bilaminate layer V containing aggregates of pyramidal cells. Layer V is thinner and more trilaminate than in 13m. Does not have outer and inner sublaminae broken up into neuron aggregates. (Carmichael & Price, 1994)
Granular 2	
10o	Is more granular than 11m and 11l, but layer IV not as clear. Layer V is thinner than in 11m or 11l; contains vertical and horizontal striations in layer V, and layer V is thinner than 11l and 11m. (Carmichael & Price, 1994)
10m	Has completely developed II and IV; has horizontal and vertical striations in layer V. Layer IV is more granular than 11m and 11l but not well demarcated, thin layer V with radial striations. (Carmichael & Price, 1994)
12m	Has completely developed II and IV; has clearly sublaminated layer V. Is more granular than 12r, 13l, and 12o. (Carmichael & Price, 1994)
12l	Has completely developed layers II and IV; has prominent/sharp sublamination of layer V. (Carmichael & Price, 1994)
45	Well developed layer IV with medium sized layer V (also has distinct and uniquely thick layer III). (Petrides & Pandya, 2001)
Granular 3	
8Av	Layer IV is broad and densely packed with small neurons (Layer II is also developed and densely packed). Layer V is less dense, but is bilaminate. Resembles 8Ad, but layer IV is broader, and layer III pyramidal neurons are more densely packed. (Petrides & Pandya, 1999)
8Ad	Layer IV is broad and densely packed with small neurons (Layer II is also developed and densely packed). Layer V is less dense, but is bilaminate. Resembles 8Av, but layer IV is less broad, and layer III pyramidal neurons are less densely packed. (Petrides & Pandya, 1999)
46	Layer IV is well developed; layer V is sublaminated (layer Va has small number of deeply stained cells and layer Vb blends with layer VI). (Petrides & Pandya, 1999)
9/46d	Similar features as 46, but layer III has large and darkly stained pyramidal neurons; Located dorsally. (Petrides & Pandya, 1999)
9/46v	Similar features as 46, but layer III has large and darkly stained pyramidal neurons; Located ventrally. (Petrides & Pandya, 1999)

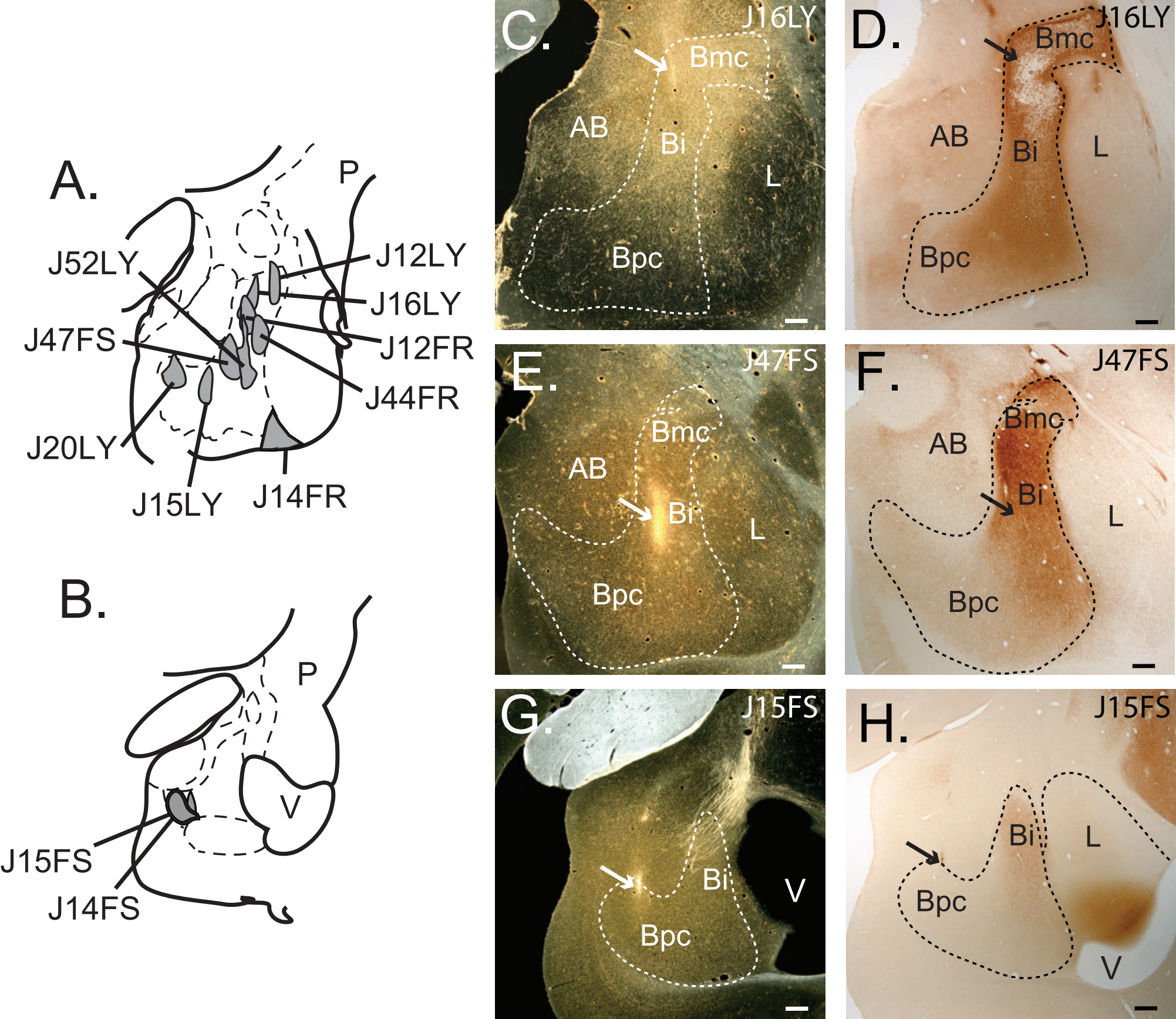
A.
P
J52LY
J12LY
J16LY
J47FS
J12FR
J44FR
J20LY
J15LY
J14FR
B.
P
V
J15FS
J14FS
C.
J16LY
Bmc
AB
Bi
L
Bpc
D.
J16LY
Bmc
AB
Bi
L
Bpc
E.
J47FS
Bmc
AB
Bi
L
Bpc
F.
J47FS
Bmc
AB
Bi
L
Bpc
G.
J15FS
Bi
V
Bpc
H.
J15FS
Bi
L
Bpc
V

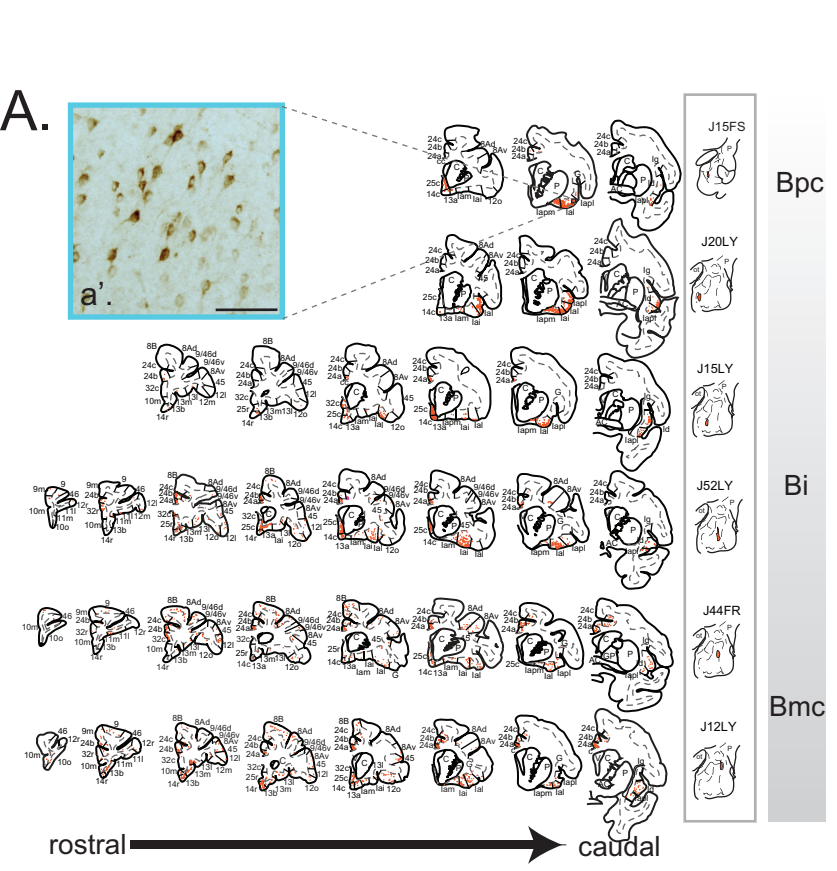
A.
a'.
J15FS
J20LY
J15LY
J52LY
J44FR
J12LY
Bpc
Bi
Bmc
rostral
caudal

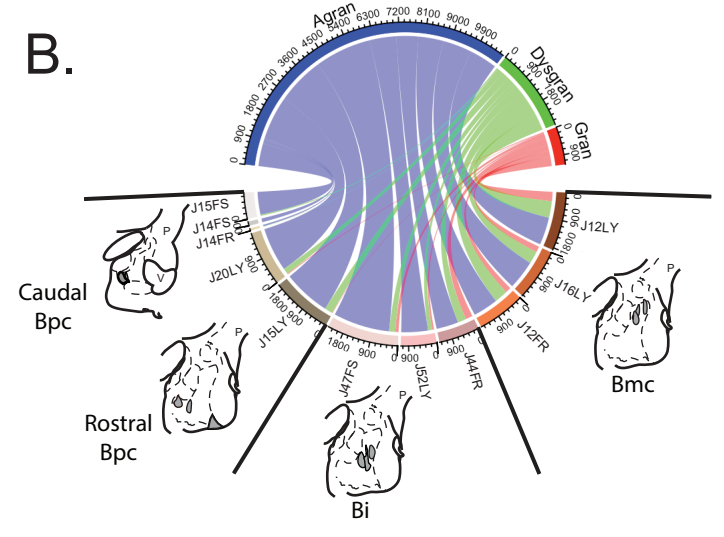
B.
Agran
Dysgran
Gran
J15FS
J14FS
J14FR
J20LY
J15LY
J47FS
J52LY
J44FR
J12FR
J16LY
J12LY
Caudal Bpc
Rostral Bpc
Bi
Bmc

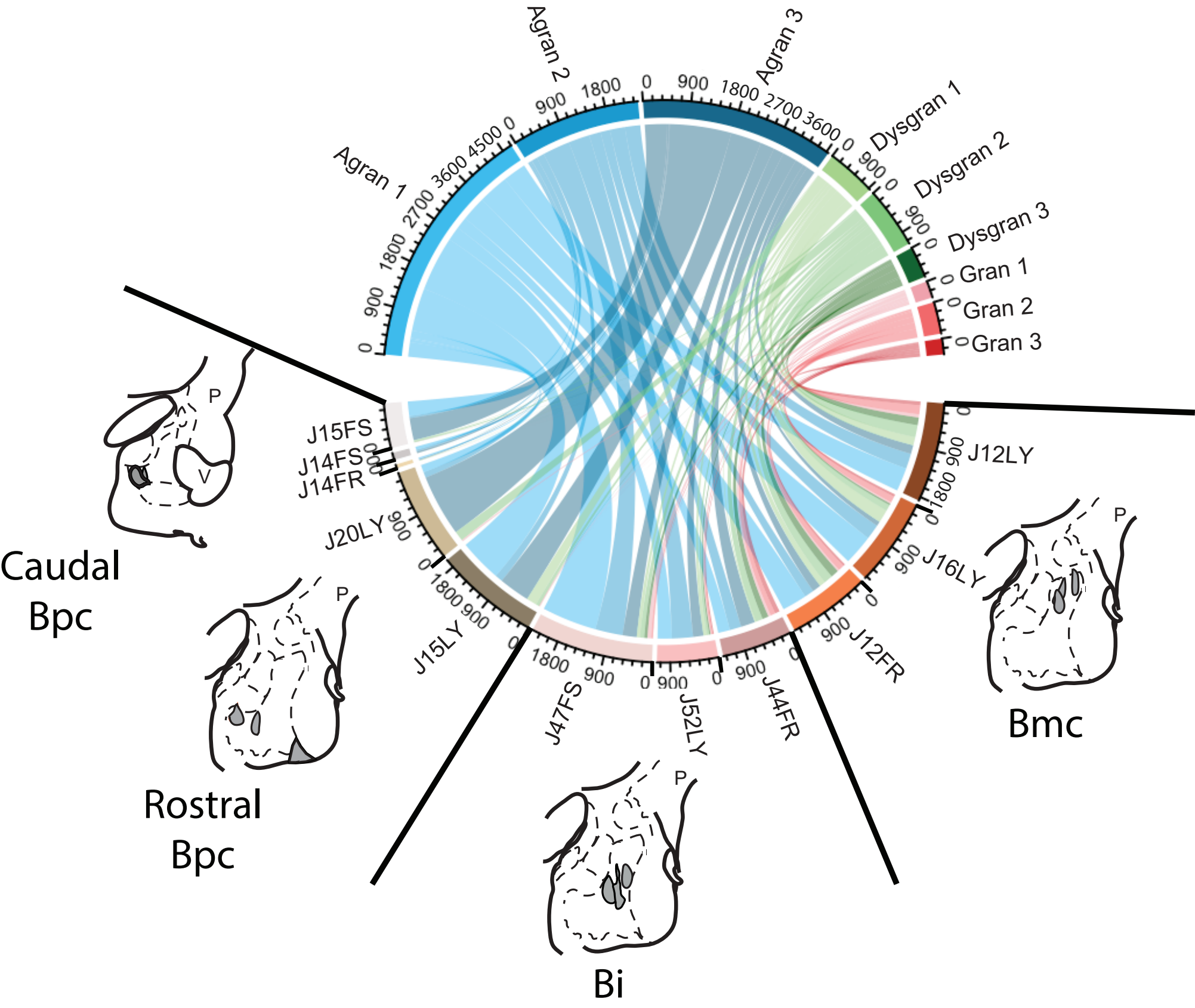
Agran 1
Agran 2
Agran 3
Dysgran 1
Dysgran 2
Dysgran 3
Gran 1
Gran 2
Gran 3
J15FS
J14FS
J14FR
J20LY
J15LY
J47FS
J52LY
J44FR
J12FR
J16LY
J12LY
Caudal Bpc
Rostral Bpc
Bi
Bmc
P
V

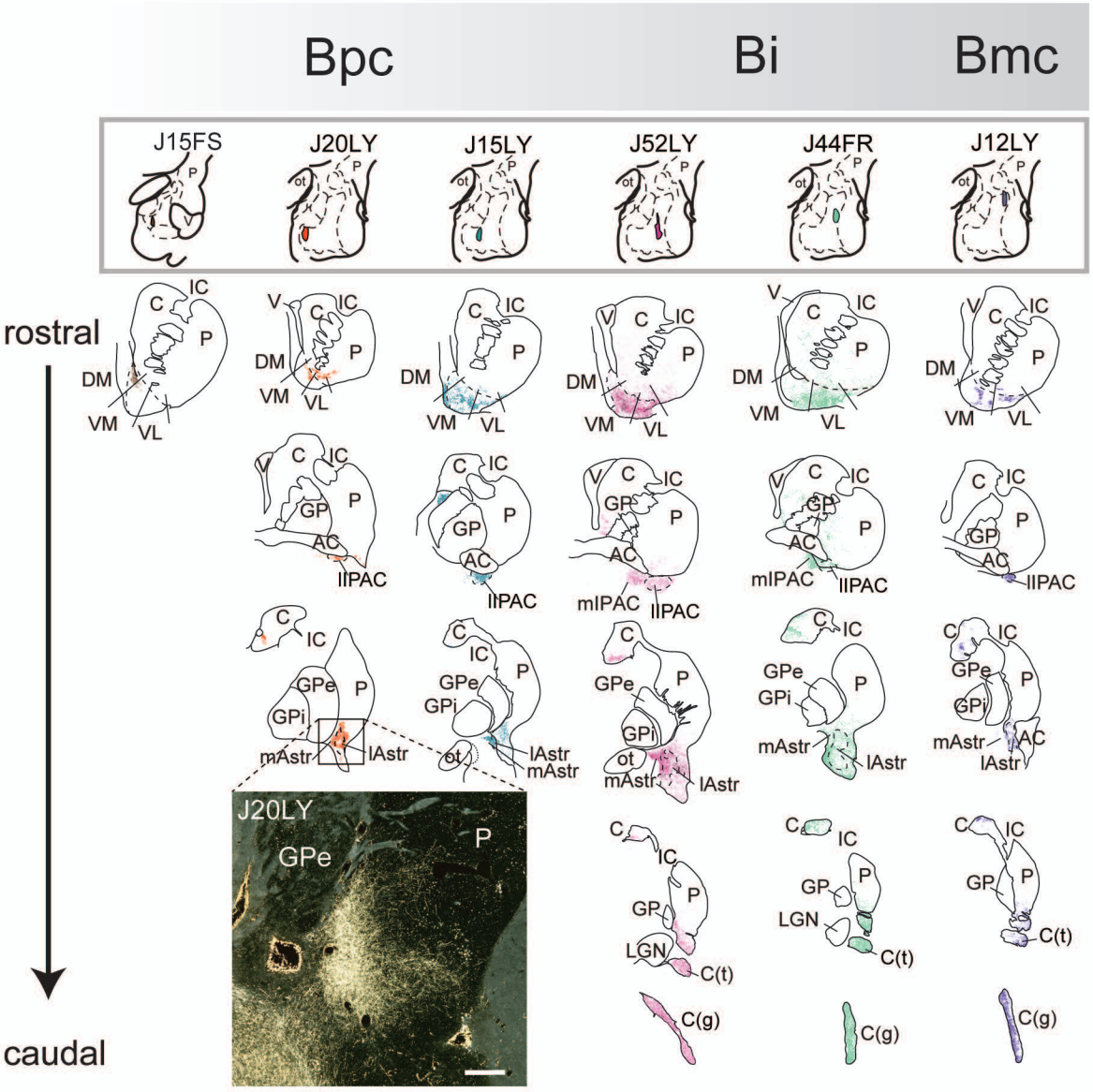

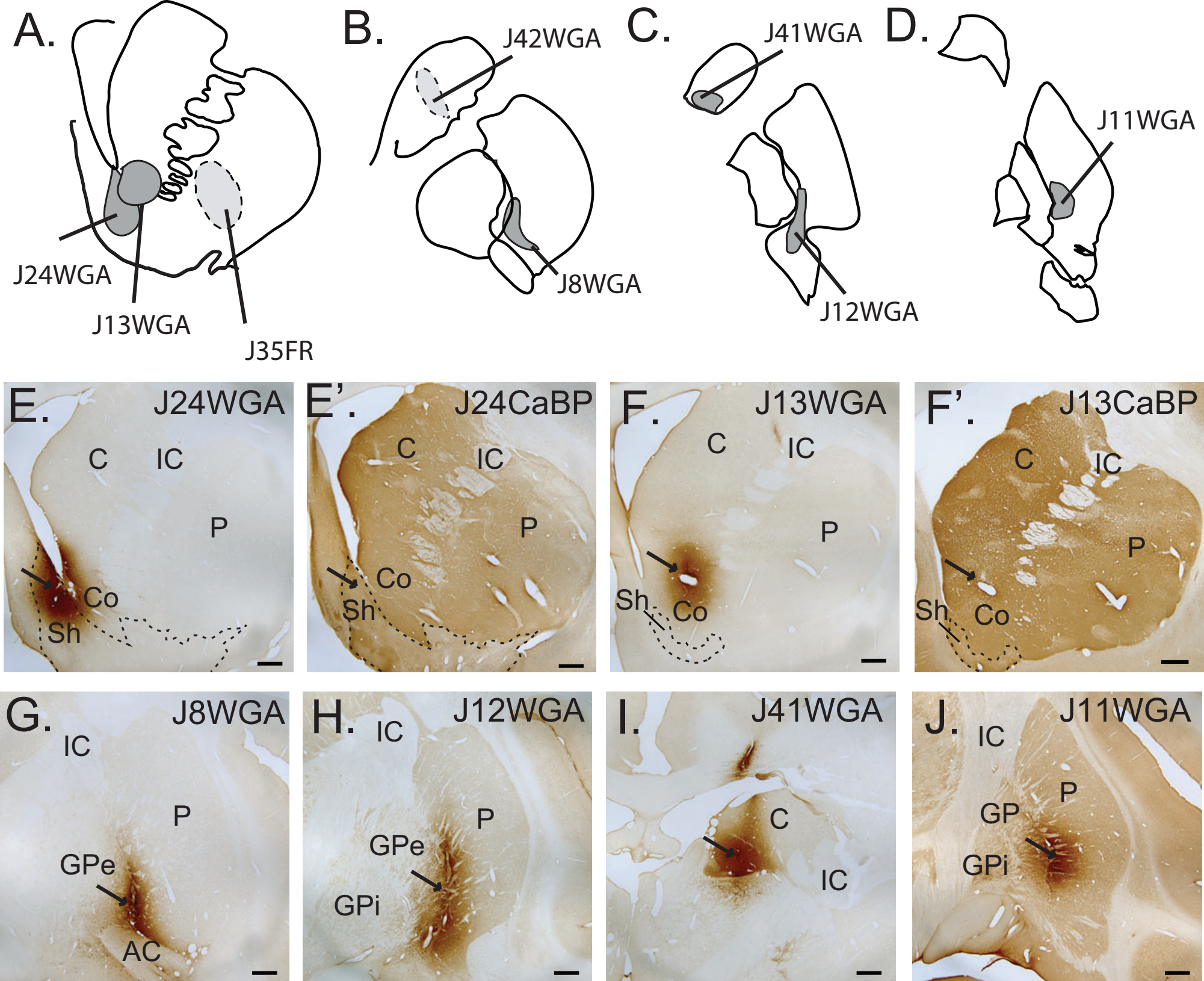
A.
J24WGA
J13WGA
J35FR
B.
J42WGA
J8WGA
C.
J41WGA
J12WGA
D.
J11WGA
E.
J24WGA
C
IC
P
Co
Sh
E'.
J24CaBP
C
IC
P
Co
Sh
F.
J13WGA
C
IC
P
Sh
Co
F'.
J13CaBP
C
IC
P
Sh
Co
G.
J8WGA
IC
P
GPe
AC
H.
J12WGA
IC
P
GPe
GPi
I.
J41WGA
C
IC
J.
J11WGA
IC
P
GP
GPi

A.

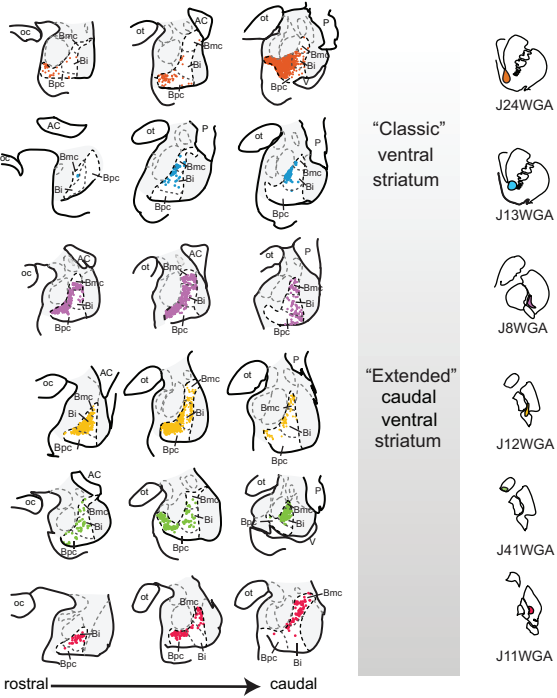

“Classic” ventral striatum

“Extended” caudal ventral striatum

B.

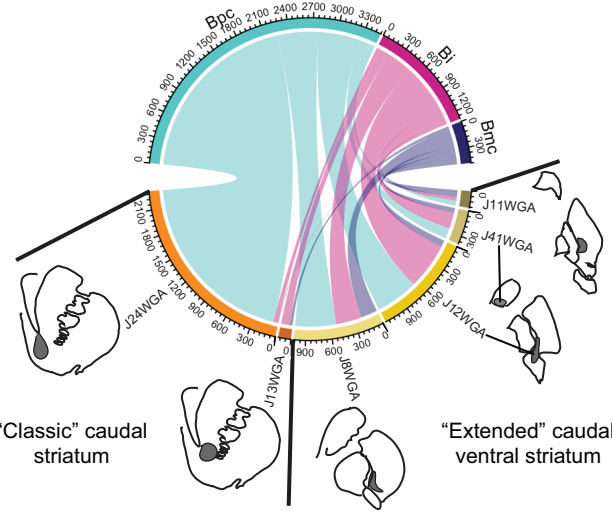

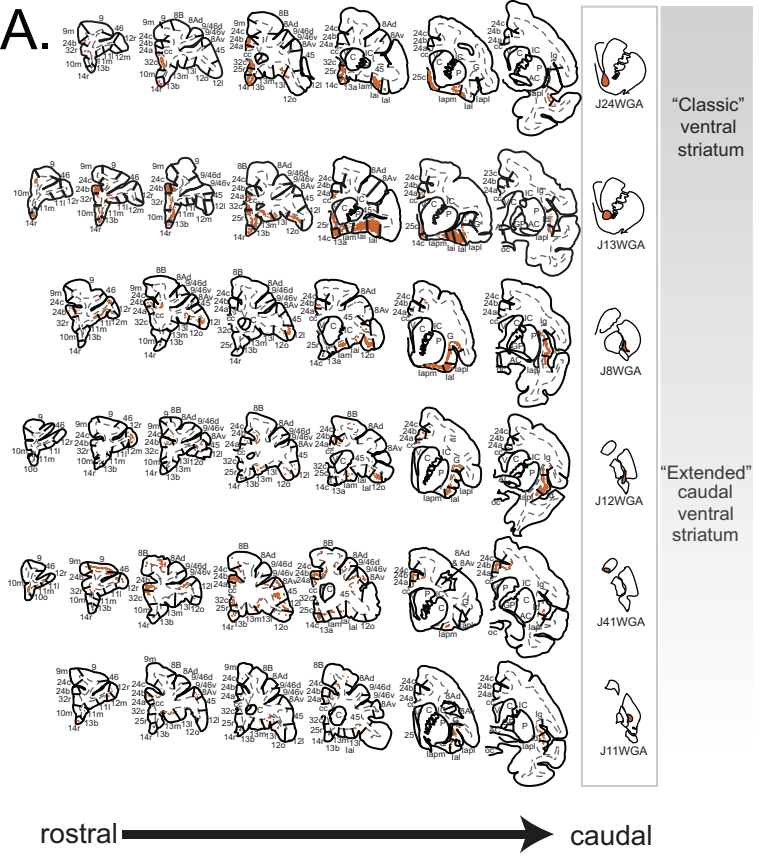
A.
J24WGA
J13WGA
J8WGA
J12WGA
J41WGA
J11WGA
"Classic" ventral striatum
"Extended" caudal ventral striatum
rostral
caudal

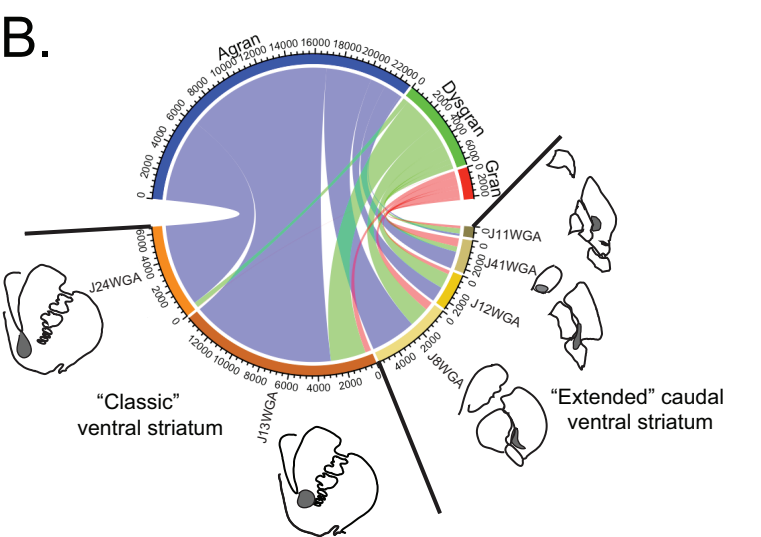
B.
Agran
Dysgran
Gran
J11WGA
J41WGA
J12WGA
J8WGA
J13WGA
J24WGA
"Classic" ventral striatum
"Extended" caudal ventral striatum

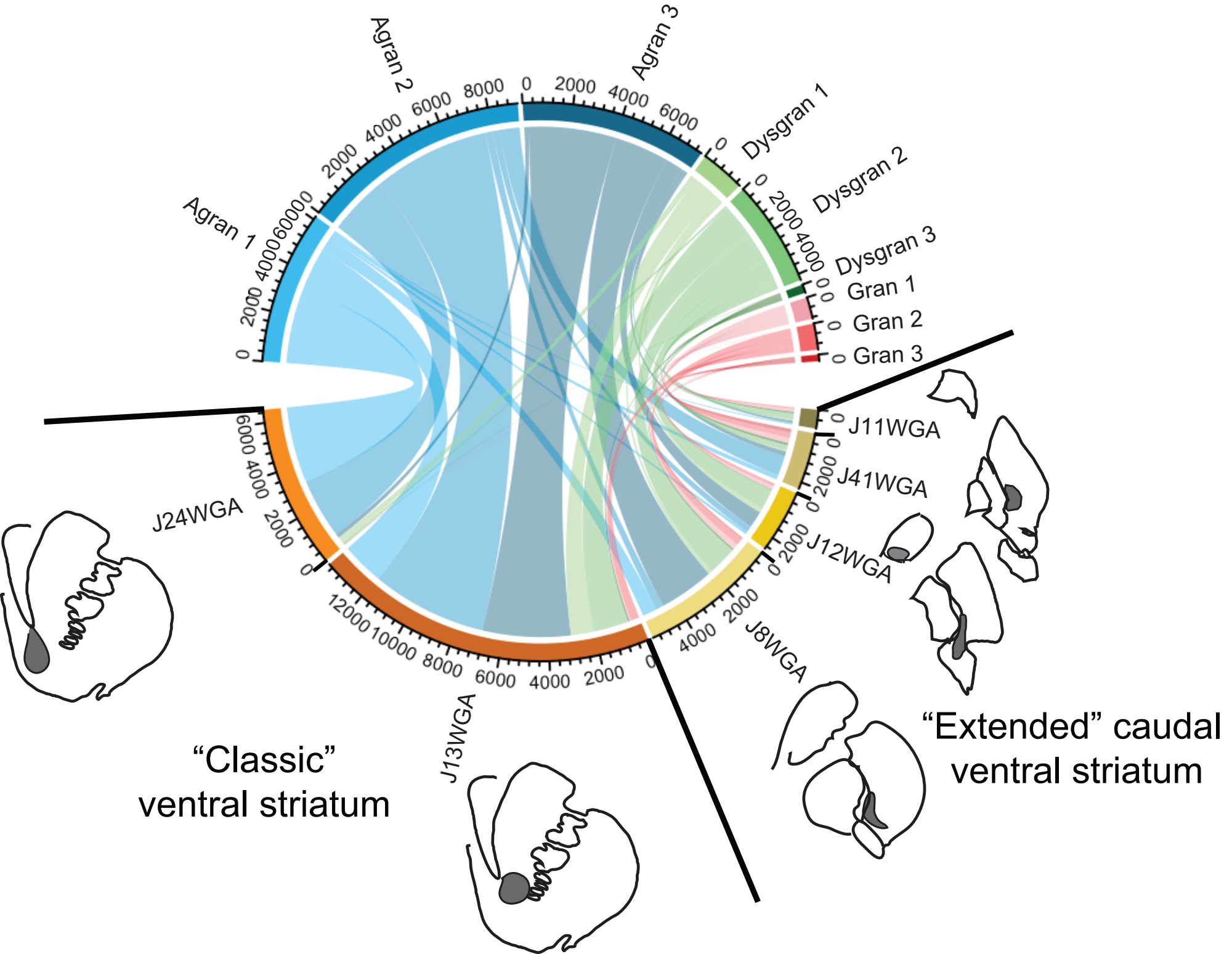
Agran 1
Agran 2
Agran 3
Dysgran 1
Dysgran 2
Dysgran 3
Gran 1
Gran 2
Gran 3
J11WGA
J41WGA
J12WGA
J8WGA
J13WGA
J24WGA
"Classic" ventral striatum
"Extended" caudal ventral striatum

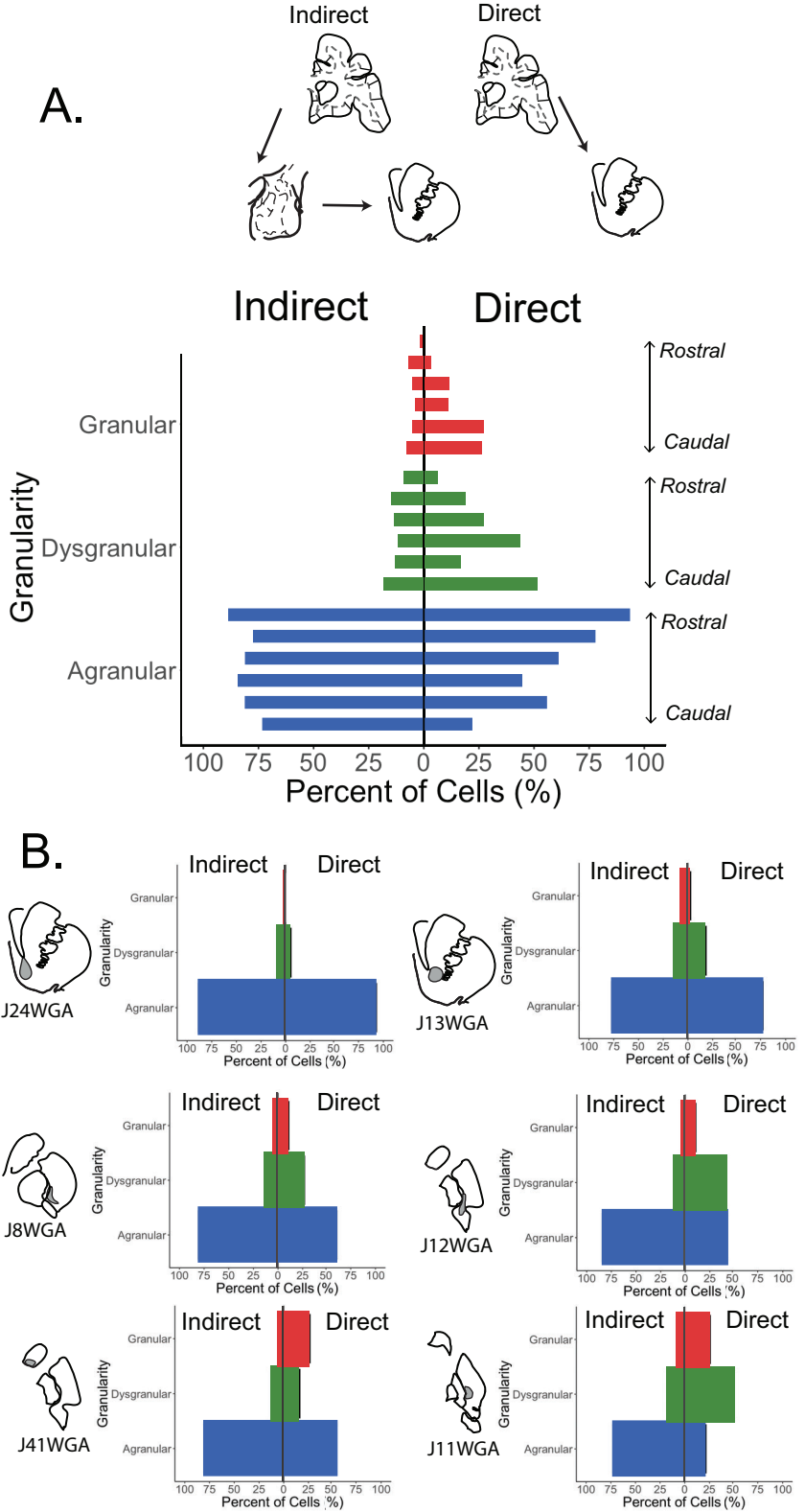
A.
Indirect
Direct
Indirect
Direct
Granular
Dysgranular
Agranular
Granularity
Rostral
Caudal
Rostral
Caudal
Rostral
Caudal
100 75 50 25 0 25 50 75 100
Percent of Cells (%)
B.
J24WGA
J13WGA
J8WGA
J12WGA
J41WGA
J11WGA
Indirect
Direct
Granular
Dysgranular
Agranular
Granularity
100 75 50 25 0 25 50 75 100
Percent of Cells (%)

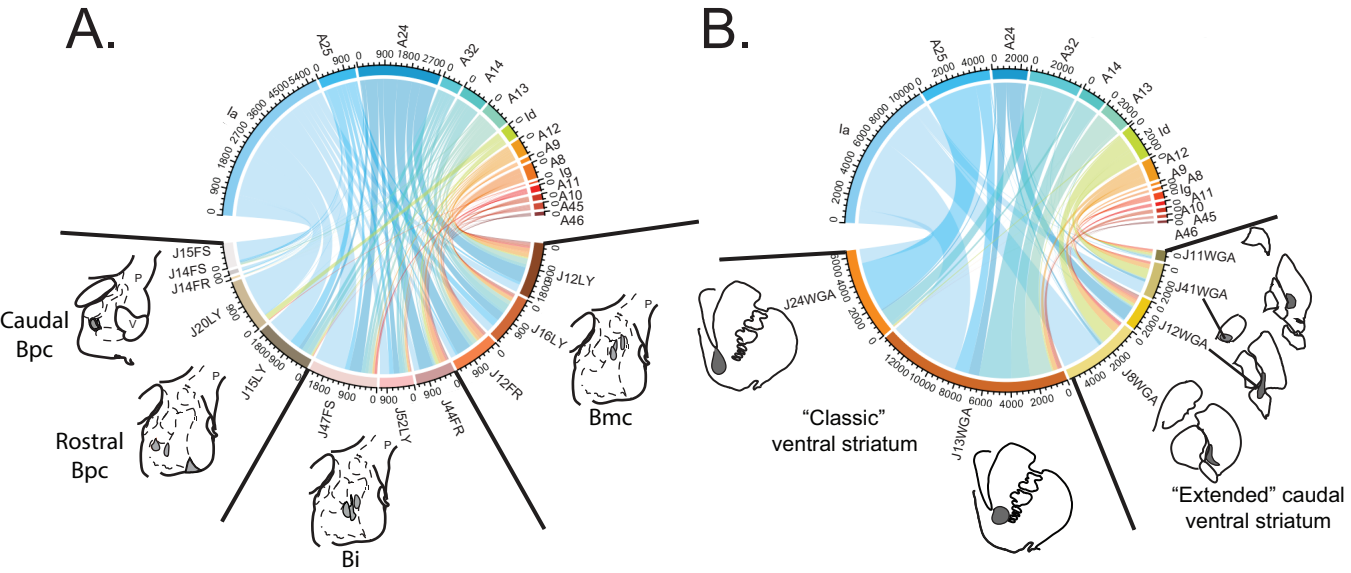
A.
B.
A25
A24
A32
A14
A13
Id
A12
A9
A8
Ig
A11
A10
A45
A46
Ia
J15FS
J14FS
J14FR
J20LY
J15LY
J47FS
J52LY
J44FR
J12FR
J16LY
J12LY
Caudal Bpc
Rostral Bpc
Bi
Bmc
J24WGA
J11WGA
J41WGA
J12WGA
J8WGA
J13WGA
"Classic" ventral striatum
"Extended" caudal ventral striatum

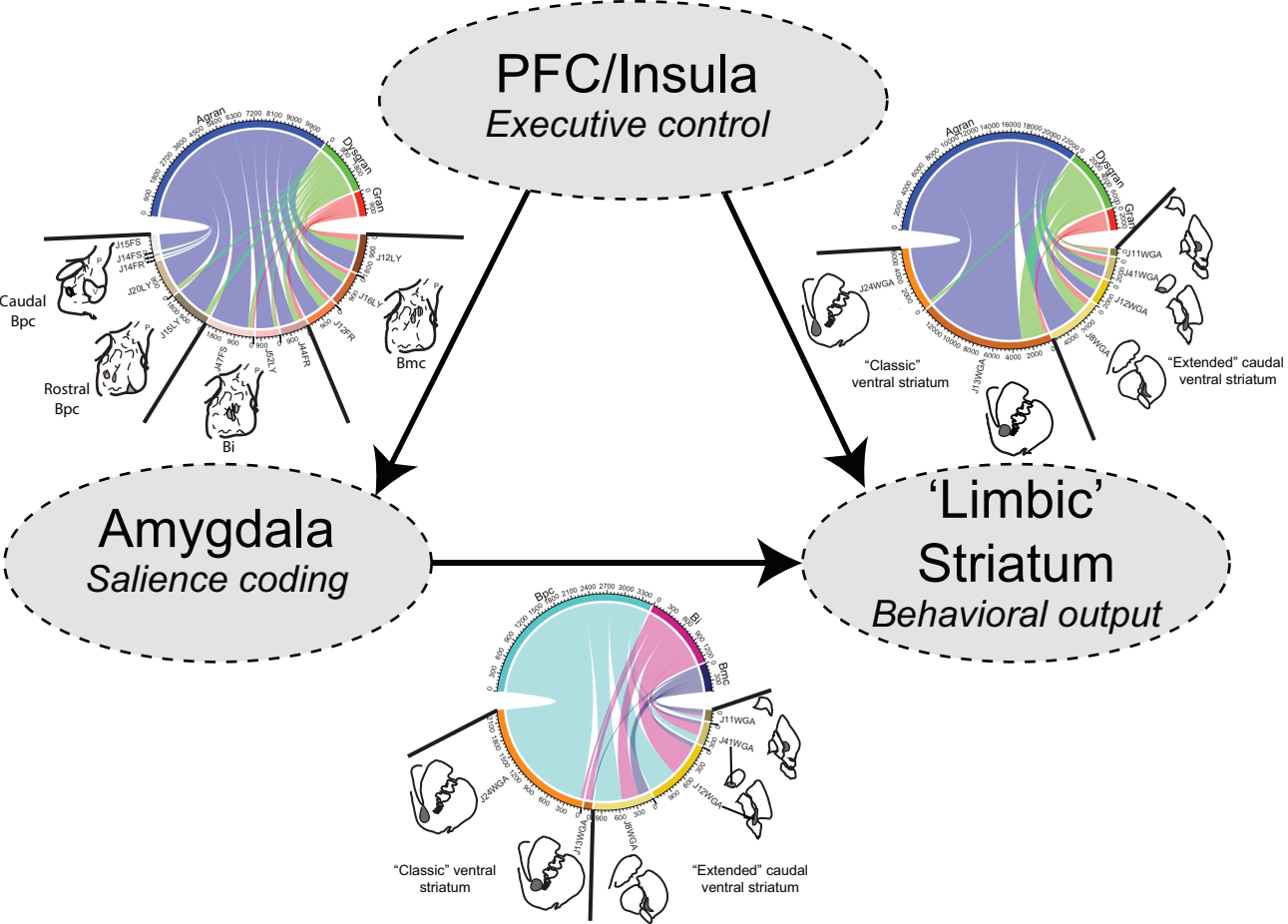
PFC/Insula
Executive control
Amygdala
Salience coding
'Limbic'
Striatum
Behavioral output
Agran
Dysgran
Gran
J15FS
J14FS
J14FR
J20LY
J15LY
J47FS
J52LY
J46FR
J12SFR
J16LY
J12LY
Caudal
Bpc
Rostral
Bpc
Bi
Bmc
J24WGA
J13WGA
J28WGA
J12WGA
J41WGA
J11WGA
"Classic"
ventral striatum
"Extended" caudal
ventral striatum
Bpc
Bi
Bmc